AGU PUBLICATIONS

JGR

Journal of Geophysical Research: Oceans

RESEARCH ARTICLE

10.1002/2016JC012636

Transport and thermohaline variability in Barrow Canyon on the Northeastern Chukchi Sea Shelf

Thomas J. Weingartner[1], Rachel A. Potter[1], Chase A. Stoudt[1], Elizabeth L. Dobbins[1], Hank Statscewich[1], Peter R. Winsor[1], Todd D. Mudge[2], and Keath Borg[2]

[1]Institute of Marine Science, University of Alaska, Fairbanks, Alaska, USA, [2]ASL Environmental Sciences, Inc., Victoria, British Columbia, Canada

Key Points:
- Transport variations are controlled by Chukchi and Bering seas winds, which allow statistically robust transport hindcasts
- Hindcasts define an climatological annual transport cycle that is downcanyon in summer, upcanyon in fall, and zero in winter
- Canyon water properties and upcanyon and downcanyon transport event durations vary seasonally

Correspondence to:
T. J. Weingartner,
tjweingartner@alaska.edu

Citation:
Weingartner, T. J., R. A. Potter, C. A. Stoudt, E. L. Dobbins, H. Statscewich, P. R. Winsor, T. D. Mudge, and K. Borg (2017), Transport and thermohaline variability in Barrow Canyon on the Northeastern Chukchi Sea Shelf, *J. Geophys. Res. Oceans*, *122*, doi:10.1002/2016JC012636.

Received 15 DEC 2016
Accepted 21 MAR 2017
Accepted article online 28 MAR 2017

Abstract We used a 5 year time series of transport, temperature, and salinity from moorings at the head of Barrow Canyon to describe seasonal variations and construct a 37 year transport hindcast. The latter was developed from summer/winter regressions of transport against Bering-Chukchi winds. Seasonally, the regressions differ due to baroclinicity, stratification, spatial, and seasonal variations in winds and/or the surface drag coefficients. The climatological annual cycle consists of summer downcanyon (positive and toward the Arctic Ocean) transport of ~0.45 Sv of warm, freshwaters; fall (October–December) upcanyon transport of ~−0.1 Sv of cooler, saltier waters; and negligible net winter (January–April) mass transport when shelf waters are saline and near-freezing. Fall upcanyon transports may modulate shelf freezeup, and negligible winter transports could influence winter water properties. Transport variability is largest in fall and winter. Daily transport probability density functions are negatively skewed in all seasons and seasonal variations in kurtosis are a function of transport event durations. The latter may have consequences for shelf-basin exchanges. The climatology implies that the Chukchi shelf circulation reorganizes annually: in summer ~40% of the summer Bering Strait inflow leaves the shelf via Barrow Canyon, but from fall through winter all of it exits via the western Chukchi or Central Channel. We estimate a mean transport of ~0.2 Sv; ~50% less than estimates at the mouth of the canyon. Transport discrepancies may be due to inflows from the Beaufort shelf and the Chukchi shelfbreak, with the latter entering the western side of the canyon.

Plain Language Summary Barrow Canyon is a major avenue by which water flows northward from the Pacific Ocean, across the Chukchi Sea, and into the Arctic Ocean. Understanding the water flow through the canyon and its variability deepens our understanding of the Chukchi Sea and its connections to the Arctic Ocean. We used 5 years of direct current measurements to develop transport predictions based on winds. The regressions allow us to hindcast daily Barrow Canyon transports from 1979–2015. The 37-year hindcast record is used to better understand the annual cycle of transport over the northeastern Chukchi Sea. The results imply that the Chukchi Sea circulation field undergoes a major re-organization on an annually. In summer the transport is a maximum and towards the Arctic Ocean, however in fall, the transport is weak but from the Arctic Ocean onto the shelf. The mean winter transport is negligible. The results have important implications for water mass formation processes on the Chukchi Sea shelf and on the movement of Pacific Waters into the Arctic Ocean.

1. Introduction

Pacific-derived waters flowing northward through Bering Strait cross the Chukchi Sea along three principal pathways: Barrow Canyon on the northeastern shelf, Herald Valley in the west, and the Central Channel over the central shelf. The Pacific inflow is a substantial source of nutrients and carbon [*Walsh et al*., 1989; *Codispoti et al*., 2005; *Nishino et al*., 2011], heat [*Steele et al*., 2004; *Shimada et al*., 2006; *Woodgate et al*., 2010; *Corlett and Pickart*, 2017], and freshwater [*Yamamoto-Kawai et al*., 2008] to the polar basin. The partitioning of the inflow among these channels is poorly understood, although it is clear that the transport variations are largely associated with winds over the Pacific sector of the Arctic [*Winsor and Chapman*, 2004; *Spall*, 2007; *Danielson et al*., 2014]. Changes in Pacific water fluxes through these channels can affect rates and patterns of ice processes, biological production, and the potential vorticity (PV) structure of the adjacent

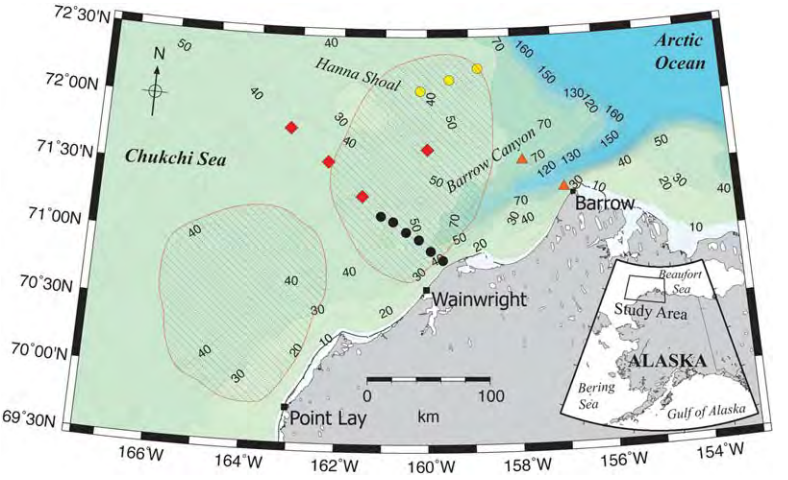

Figure 1. Bathymetric map of the northeastern Chukchi Sea showing mooring locations. The 2010–2012 arrays of six moorings are shown with black dots and consist of moorings BC1 (closest to the coast) through BC6. Additional moorings, summarized in the discussion, are shown using colored symbols. HFRs were located in Point Lay, Wainwright, and Barrow. The striped regions encapsulate that portion of the HFR mask containing 50% or more good data.

shelfbreak and slope. The latter has consequences on shelf-basin exchange processes [*Spall et al*., 2008] and the circumpolar slope circulation [*Spall*, 2013]. Herein, we use a 5 year time series of moored measurements to examine hydrographic and transport variability at the head of Barrow Canyon and to construct a transport climatology using 37 years of regional winds.

Barrow Canyon extends ∼220 km from its head, north of Wainwright, to its mouth on the continental slope (Figure 1). Bottom depths increase linearly along its length from 50 to 300 m. Between Wainwright and Barrow (∼140 km), the canyon is bounded by the Alaskan coast; whereas north of Pt. Barrow, the canyon delimits the western end of the Beaufort Sea shelf. The western wall of the canyon adjoins a broad, shallow (40–60 m) bench that extends ∼80 km westward to Hanna Shoal. In cross section, the canyon is nearly U-shaped, with the width varying from ∼40 km at its head to ∼60 km at its mouth (based on the distance between the 70 m isobaths on either side of the canyon mouth). The aspect ratio (δ), the ratio of the cross-canyon to along-canyon length scales, is ∼0.3.

Most submarine canyons that incise shelfbreaks lie athwart the prevailing along-shelf currents that control the canyon circulation [e.g., *Allen and Durrieu de Madron*, 2009]. Barrow Canyon shares this feature insofar as the flow over the Chukchi/Beaufort shelfbreak is transverse to the canyon axis [e.g., *Mountain et al*., 1976; *Pickart*, 2004; *Nikolopoulos et al*., 2009]. In contrast to most canyons, currents along the longitudinal axis of Barrow Canyon are swifter than the transverse flows nearer its mouth and are strongly influenced by Bering and Chukchi shelf processes operating to the south. These shelf regions are also the source of summer and fall waters comprising the horizontally and vertically structured along-canyon flow [*Pickart et al*., 2005; *Shroyer and Plueddemann*, 2012]. The contributing water masses include moderately salty Bering Sea Water, fresh, warm Alaskan Coastal Water (ACW) [*Coachman et al*., 1975], near-freezing, saline winter-formed waters (WW) derived from ice production, and cool, dilute ice-melt waters (MW).

The most comprehensive set of long-term transport measurements in Barrow Canyon is by *Itoh et al*. [2012, 2013]. They used three moorings at the mouth of the canyon to estimate seasonal and interannual variations in canyon transports of mass, heat, and freshwater from 2000 to 2008. Their moorings were deployed at 10 km intervals, from east to west, on the 80, 250, and 150 m isobaths, respectively. They estimated a mean average transport of 0.45 Sv northeastward (which with the convention adopted in this paper is the downcanyon or positive flow direction) and into the Arctic Ocean. This flow opposes the mean northeasterly winds and is a consequence of the Pacific-Arctic pressure gradient that is also responsible for the mean northward transport in Bering Strait. *Itoh et al*. [2013] find that the flow varies seasonally and in-phase with the annual cycle of Bering Strait transport; i.e., maximum downcanyon transport occurs in summer, and minimum transport occurs in winter. In accordance with previous studies [*Aagaard and Roach*, 1990; *Münchow and Carmack*, 1997; *Weingartner et al*., 1998; *Pickart et al*., 2005; *Woodgate et al*., 2005a; *Itoh et al*., 2012],

they find that transport variations are primarily wind-forced, include reversals, have magnitudes of ~0.5–1.0 Sv, and durations of one to many days.

Our measurements, made at the head of Barrow Canyon ~190 km southwest (upcanyon) of the arrays discussed by *Itoh et al*. [2013], were part of a larger program to examine connections between Barrow Canyon and the northeastern shelf in a region contemplated for offshore oil development. Section 2 describes the data sets. Section 3 examines kinematic features and transport variability derived from the observations. These data and regional winds are used to hindcast a 37 year (1979–2015) transport record. This section also examines the hydrographic properties in relation to circulation variability. Section 4 examines why our transports differ from *Itoh et al*.'s [2013] values and discusses potential implications of our findings on the Chukchi and Beaufort shelves and slopes. Section 5 summarizes the paper.

2. Methods

2.1. Moorings

From August 2010 to September 2012, six moorings (BC1 inshore to BC6 offshore), spaced ~13 km apart, spanned the head of Barrow Canyon (Figure 1). Each mooring contained an upward looking 300 or 600 kHz Teledyne ADCP and a temperature/conductivity/pressure (TCP) recorder (Seabird SBE-37 or SBE-19). Moorings BC-2–BC-5 included bottom-tracking for measuring ice keel depths and ice drift. Bottom-tracking was inactive on BC-1 and BC-6 because these included directional wave firmware (wave data are not discussed here). The TCP and ADCP were housed in a float situated ~4 m above bottom and sampled hourly. BC1, nearest the coast, was deployed in a water depth of 31 m with its instruments mounted 1 m above the bottom in a SeaSpider frame. This design minimized damage from nearshore ice keels that can exceed 25 m depth. After recovering the array in September 2012, we deployed a single mooring (BC2) in succeeding years. We will show that BC2 provides statistically valid estimates of along-canyon transport, so BC2 data served as a proxy for transport from September 2012 to early August 2015. Table 1 lists positions, depths, and period of record for each mooring. There were several gaps in the mooring data due to premature failure of the ADCP on mooring BC2. As explained below, we filled some of these gaps with other data.

To provide context over a wider area of the shelf, we obtained mooring data supported by other programs. The red diamonds in Figure 1 indicate the locations of oil industry-sponsored moorings described by *Mudge*

Table 1. Mooring Positions and Depths for the Barrow Canyon (BC) Array and Locations of NARR Wind Grid Points

Mooring Name	Latitude (°N)	Longitude (°W)	Bottom Depth (m)	ADCP Depth (m)	ADCP Period of Record
2010–2011					
BC1	70.85	−159.67	30.1	29	18 Aug to 26 Aug
BC2	70.92	−159.94	52.3	49	17 Aug to 20 Aug
BC3	71.00	−160.21	53.3	48.5	17 Aug to 26 Aug
BC4	71.06	−160.49	49.3	45	17 Aug to 26 Aug
BC5	71.13	−160.79	49.5	45.5	17 Aug to 26 Aug
BC6	71.17	−161.07	46.6	43	18 Aug to 26 Aug
2011–2012					
BC1	70.85	−159.67	30.1	29	30 Aug to 7 Jul
BC2	70.92	−159.94	52.3	49	30 Aug to 4 May
BC3	71.00	−160.21	53.3	48.5	30 Aug to 4 July
BC4	71.06	−160.49	49.3	45	30 Aug to 19 Jul
BC5	71.13	−160.79	49.5	45.5	30 Aug to 3 May
BC6	71.17	−161.07	46.6	43	30 Aug to 31 Oct 2011
2012–2013					
BC2	70.92	−159.94	52.3	49	9 Sep to 13 Aug
2013–2014					
BC2	70.92	−159.94	52.3	49	11 Sep to 24 Sep
2014–2015					
BC2	70.92	−159.94	52.3	49	24 Sep to 10 Aug
NARR Wind Grid Points					
Geographic Area			Latitude (°N)		Longitude (°W)
Barrow Canyon (BC2)			70.92		−159.94
Bering Strait (A3)			66.33		−168.97
Northern Bering Sea (C40)			60.34		−169.02

et al. [2015]. The yellow circles are three moorings deployed northeast of Hanna Shoal (supported by the Bureau of Ocean Energy Management), and the two orange triangles are moorings (courtesy of S. Okkonen) spanning the canyon east of Barrow.

2.2. High-Frequency Radars (HFR)

During the open water seasons of 2010–2014, we measured hourly surface currents (upper 2 m) at 6 km horizontal resolution in the northeast Chukchi Sea using ~5 MHz HFRs (CODAR Ocean Sensors). Subsets of these data fill gaps in the transport time series. Field sites were located in the villages of Point Lay, Barrow, and Wainwright (Figure 1), which allowed collecting surface current data nominally within 180 km of the coast. An additional system was deployed at Cape Simpson (Figure 15) in 2013 and paired with the Barrow system to map currents in the western Beaufort Sea and over the mouth of the canyon. HFR calibrations were applied following [*Barrick and Lipa*, 1986; *Kohut and Glenn*, 2003], and HFR data were processed according to *Weingartner et al*. [2013a].

2.3. Winds

Wind and sea level pressure (SLP) estimates were obtained from NOAA's North American Regional Reanalysis (NARR) models [*Mesinger et al*., 2006] at grid points near the Barrow Canyon mooring array (BC2), Bering Strait, and the northern Bering Sea (Table 1). Both variables have space and time resolutions of 32 km and 3 h, respectively.

3. Results

3.1. Kinematic Description

All six moorings from the 2010 to 2011 array provided year-long data sets. These data, low-pass filtered to remove diurnal and shorter period fluctuations, are used to describe kinematic features of the flow at the head of the canyon. The record-length mean vertically averaged velocity vectors and variance ellipses (Figure 2a) show that between moorings BC1 and BC3, the mean flow was northeastward at between 0.1 and 0.2 m s^{-1}, with maximum values at BC2. Farther offshore (moorings BC4–BC6), the mean vectors were east-southeastward and onshore at ~0.1 m s^{-1}. The vectors imply that upon entering the western side of the canyon head the mean flow veered counterclockwise by ~25° over a radius of 13 km (between BC4 and BC3), so the bulk of the alongshore flow occurred within ~35 km of the coast. Ellipse orientations were alongshore polarized at the four inshore moorings (BC1–BC4; where the topographic slopes are greatest) and cross-shore polarized at the two outer moorings (BC5 and BC6). Standard deviations of the alongshore flow were three times the mean values at BC1–BC3 and twice the means at BC4–BC6. On a monthly basis, the principal axes at each site varied by less than 15°. Currents along these axes explained >95% of the current variance at moorings BC1–BC3, >90% at BC4, and >75% at mooring BC5 and BC6.

Another perspective on the velocity structure is provided by vertical sections of velocity using an alongshore and cross-shore coordinate system based on the approximate orientation of the coast between Wainwright and Barrow. In this system, positive alongshore or downcanyon velocities, u_r, are toward 56°T, and $u_r < 0$ is upcanyon toward 236°T. Positive cross-shore velocities, v_r, are offshore toward 326°T, and $v_r < 0$ is onshore toward 146°T. We classified the flow as being downcanyon or upcanyon according to the sign of u_r at ~20 m depth at BC2. (This classification scheme is satisfied by virtually any choice of depth or mooring position.) From 2010 to 2011, the u_r record (Figure 2b) indicated that the flow was generally downcanyon. Speeds were typically between 0.2 and 0.5 m s^{-1}, but, u_r often exceeded 0.5 m s^{-1}, and its maximum was ~1.0 m s^{-1}. Upcanyon currents occurred ~30% of the time, were generally swifter than downcanyon currents, and had a maximum speed of 1.2 m s^{-1}. From mid-August to September 2010 and from May to August 2011, the flow was primarily downcanyon and steady compared to the period of October 2010 to April 2011, when current speeds and variations were greater. As determined from adjacent moorings, the mean cross-canyon Rossby number ($Ro_y = \partial u_r / f \partial y$, where y is the cross-shore coordinate and f is the Coriolis parameter) was $\ll 1$, but ~20% of Ro_y magnitudes were between 0.2 and 0.4 and highest on either side of BC-2. The majority of the larger values were associated with upcanyon flows in fall indicating that, at times, the cross-shore advection of along-canyon momentum can be significant.

Figures 3a and 3b show the year-long mean vertical sections of u_r and v_r. On average, the flow was downcanyon everywhere despite the fact that the mean winds were ~2.4 m s^{-1} toward 255°T, i.e., opposite the mean

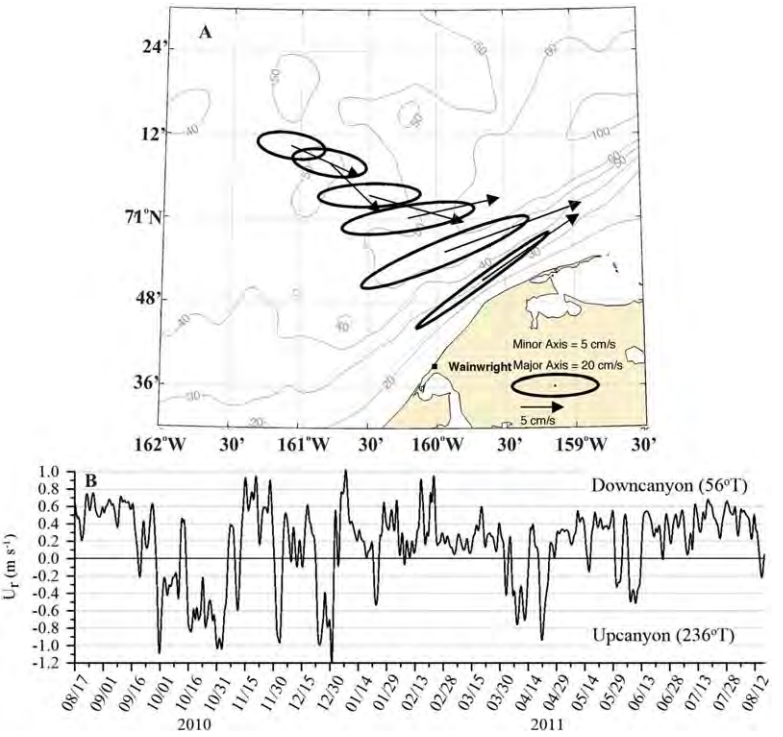

Figure 2. (a) Vertically averaged velocity vectors and variance ellipses for the moorings at the head of Barrow Canyon. Note the velocity scale change between the mean vector and the variance ellipse. (b) Time series of the along-canyon currents at 20 m depth at mooring BC2. Both figures are based on the August 2010 to August 2011 mooring records.

downcanyon flow. The u_r composite indicates an alongshore jet centered at BC2 with a maximum speed of 0.16 m s^{-1} between 20 and 40 m depth. The cross-shore flow was onshore everywhere, with the largest onshore velocities observed below 20 m depth at moorings BC4–BC6. There were two regions of onshore convergence. The first was between BC3 and BC4 where, as noted (Figure 2a), the mean onshore flow veered counterclockwise into the canyon. The second was between BC1 and BC2 and likely reflects the coastal boundary constraint.

Figures 3c and 3d (3e and 3f) are the u_r and v_r sections composited from all downcanyon (upcanyon) flow events, respectively. For both flow regimes, the along-canyon structure had three features in common. First, each included an along-canyon jet, centered at BC2, with maximum speeds in the uppermost 20 m. Second, the jets are somewhat asymmetrical with the horizontal shear slightly larger on the offshore side of the jet (between BC2 and BC3) than on the inshore side. Third, $v_r \sim \delta u_r$ in all sections, consistent with the aspect ratio. In the downcanyon case, there was little vertical shear in u_r, but considerable shear in v_r at BC1 and BC2. The v_r-distribution indicates onshore convergence between BC4 and BC1 with maximum convergence within ~20 km of the coast. The mean u_r speeds for the upcanyon-flow composite (Figure 3e) were larger than those for the downcanyon case. The vertical shear in u_r was weak ($\leq 10^{-3}$ s^{-1}) seaward of about 25 km, but substantial ($\sim 5 \times 10^{-3}$ s^{-1}) within the core of the jet. For upcanyon flow v_r (Figure 3f) consisted of offshore, vertically sheared flow everywhere, divergent between BC1 and BC2 but weakly convergent seaward of BC2.

Empirical orthogonal function (EOF) calculations indicate that the velocity fluctuations were highly coherent over the mooring array. The first EOF mode (Figures 3g and 3h) captures more than 90% of the variance in the velocity components. Mode weights for u_r were vertically uniform, greatest within 20 km of the coast, and much smaller seaward of BC4. For v_r, the amplitudes increased with depth, were greatest below 20 m at BC3, and smallest at the surface near the coast. (EOF results from 2011 to 2012 were similar.)

3.2. Transport: Observations

We computed daily and vertically averaged transports assuming uniform velocity between the topmost bin and the surface. We also estimated transports by extrapolating to the surface either the upper ocean shear

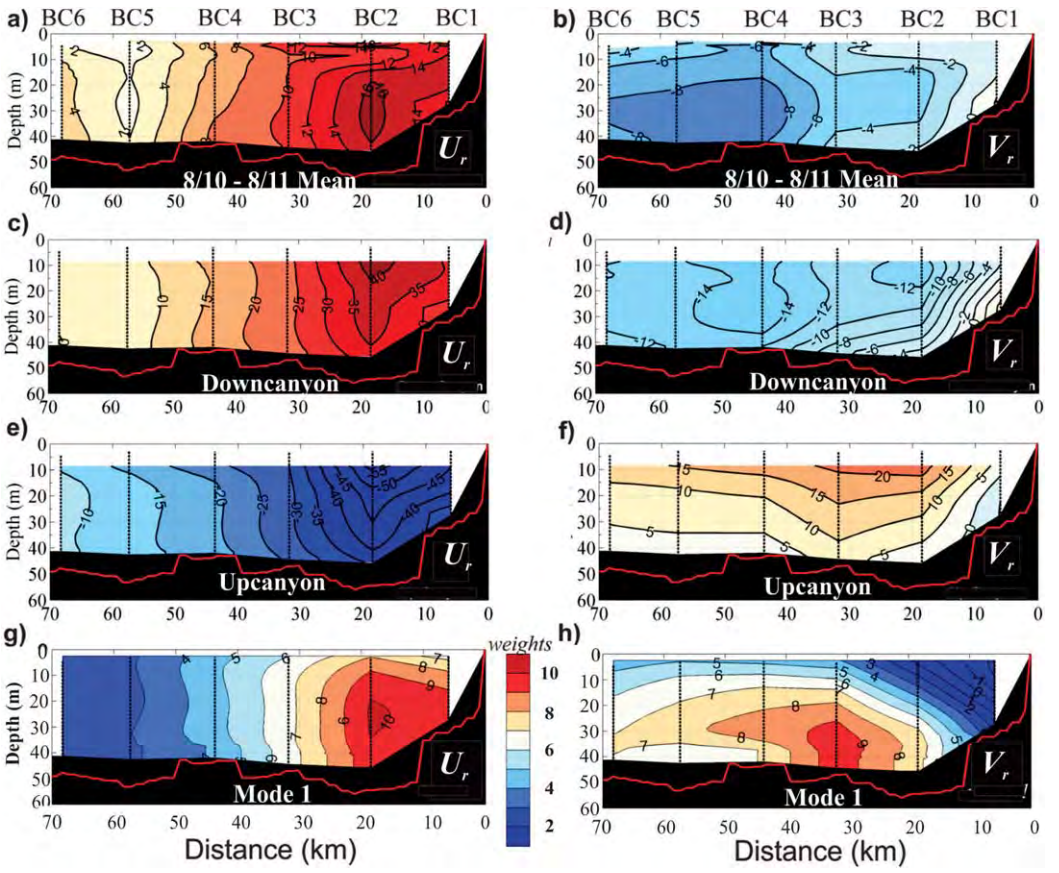

Figure 3. Vertical sections of the mean annual: (a) along-canyon, u_r and (b) cross-canyon, v_r velocities. Mean sections of (c) u_r and (d) v_r for the downcanyon case, and of (e) u_r and (f) v_r for the upcanyon case. Vertical sections of the first EOF eigenvector for (g) u_r and (h) v_r. All figures are based on the August 2010 to August 2011 period.

and/or interpolations between the uppermost measured velocity and the ice velocity. The different approaches yielded no significant differences in the transport estimates. Daily transports for 2010–2011 were then regressed against the mean daily vertically averaged u_r at BC2 and BC4. Both regressions were statistically significant at the 95% confidence level. The BC2 (BC4) regression accounted for 96% (93%) of the variance. The BC2 regression (Table 2) was used to estimate mean daily transports for the August 2011 to August 2015 period. There were several gaps due to premature ADCP failure at BC2. The BC4 regression filled the gap from 4 May to 19 July 2012 (when BC4 died). Remaining gaps were 21–29 August 2011, 19 July to 9 September 2012, and 13 August to 10 September 2013. We filled most of these gaps by regressing the vertically averaged velocity at BC2 in each year against the mean daily HFR surface velocity at grids surrounding the BC2 location. These regressions accounted for 80–90% of the BC2 transport variance in each case. Poor quality HFR returns due to drifting sea ice prevented interpolating transports during the 15 day period of 19 July to 2 August 2012. Errors in the transport estimates arise from the regressions procedures, the alongshore coordinate choice, and the neglect of transport between the coast and mooring. In aggregate we consider the uncertainty in these estimates to be between 15% and 20%.

The mean daily along-canyon winds and transport for the August 2011 to July 2015 period (Figure 4) are enormously variable. For transport, the coefficient of variation (the ratio of the standard deviation to the mean) is ~4, based on the record-length mean transport of 0.19 Sv. Mean daily values ranged from a maximum of ~1.6 Sv (11 November 2013) to a minimum of −2.6 Sv (19 January 2014). Transport event durations varied from 1 to 5 days, in which fluctuation amplitudes were frequently 0.5 Sv or greater, to episodes lasting a week or more.

Transport and along-canyon wind variations at monthly and longer time scales are shown with mean monthly values (Figure 5) along with their 95% confidence limits. (For both variables these limits were

Table 2. Row 1 Is the Linear Regression Model Used to Compute Barrow Canyon transports (T) From Mooring BC2[a]

	r^2
Linear Regression: Transport Versus Vertically Averaged Along-Canyon Current at BC2	
$T(\mathrm{Sv}) = 0.019(\pm 0.001) \cdot BC2(\mathrm{cm\,s^{-1}}) - 0.007(\pm 0.04)$	0.96
GLM: Mean Daily Winter (Oct to Apr.) Transports From Alongshore And Cross-Shore Winds[b]	
$T = 0.40(\pm 0.038) + 0.021(\pm 0.007) \cdot C40V + 0.067(\pm 0.011) \cdot A3V$ $+ 0.084(\pm 0.015) \cdot BC2U - 0.038(\pm 0.013) \cdot BC2V$	0.59
GLM: Mean Daily Summer (May to Sep) Transports From Winds[b]	
$T = 0.56(\pm 0.031) + 0.025(\pm 0.007) \cdot C40V + 0.029(\pm 0.007) \cdot A3V$ $+ 0.062(\pm 0.013) \cdot BC2U - 0.018(\pm 0.013) \cdot BC2V$	0.55

[a]Rows 2 and 3 are the winter and summer GLM models used to hindcast Barrow Canyon transport based on winds listed in Table 1 over the Bering Sea shelf (C40), Bering Strait (A3), and Barrow Canyon (BC2). Terms in parentheses are the 95% confidence limits on the model coefficients using an integral time scale of 4 days. The wind components (*V*, *U*) and lags at each site are defined in the footnote.
[b]*BC2U*: 67°T; *BC2V*: 157°T both lead transport by 1 day; *A3V*: 15°T leads transport by 1.5 days; C40V: 315°T leads transport by 2.5 days.

constructed by bootstrapping [*Efron and Tibshirani*, 1993] because both have integral time scales of ~4 days, and neither are normally distributed.) Typical monthly transport amplitudes are ~0.5 Sv, ~2.5 times the record-length mean.

In addition to month-to-month variability, there is considerable interannual variability. For example, downcanyon transport predominated from November 2010 to March 2011, while upcanyon transport dominated over the same period in 2012. Although the seasonal variability is largely masked by month-to-month variations, the mean monthly transports of Figure 5 describe an annual cycle (Figure 6a). The mean summer (May–September) transport was 0.45 Sv downcanyon, with the annual maximum of ~0.7 Sv occurring in July, whereas the mean transport from October to April was not significantly different from zero.

Seasonal transport variability is also reflected in the higher order statistics, as summarized in the summer and combined fall and winter probability density functions (pdfs; Figure 7; fall and winter were combined because their pdfs are similar.) For example, the summer variance (~0.29 Sv^2) is about half the fall/winter variance (~0.54 Sv^2). In both seasons, the transport pdfs are negatively skewed; extreme flow events are primarily

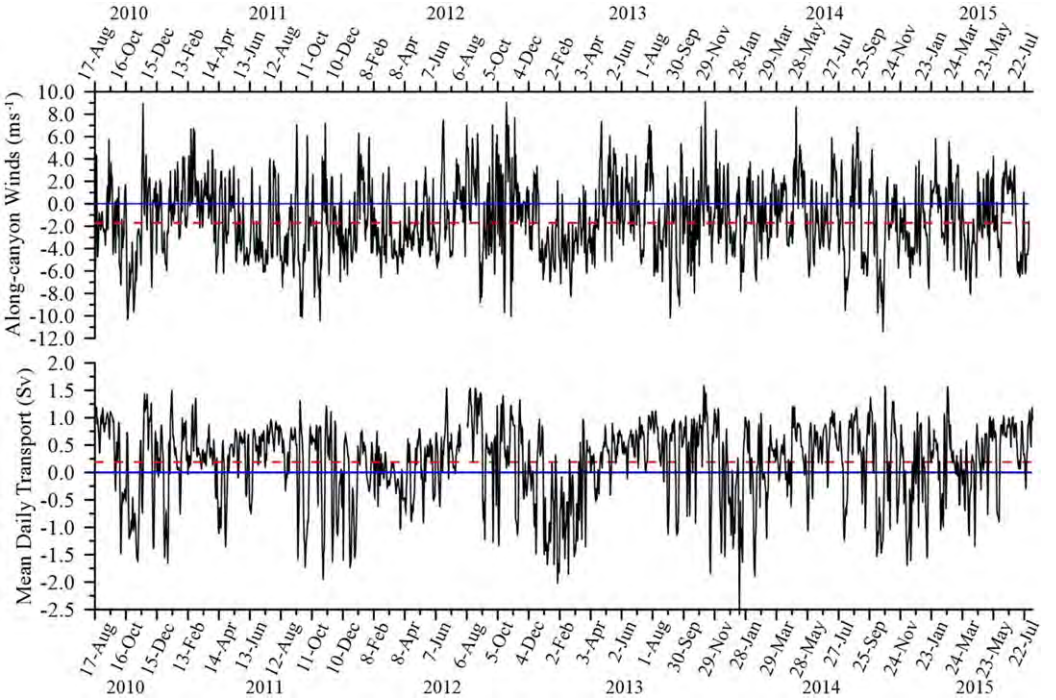

Figure 4. (top) Mean daily along-canyon winds and (bottom) transport. The dashed red line on the wind and transport time series denotes the record-length means of −1.7 m s^{-1} and 0.19 Sv, respectively.

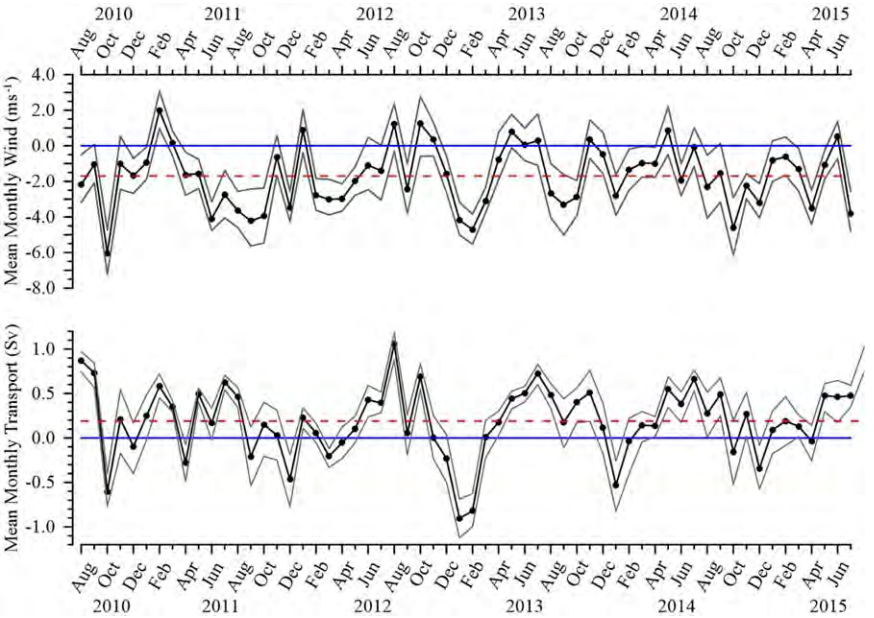

Figure 5. (top) The mean monthly along-canyon winds and (bottom) transport are denoted by black lines and dots. Crosses and gray lines delineate the bootstrapped 95% confidence limits. The dashed red lines on the transport and wind time series plots show the record-length means in transport (0.19 Sv) and along-canyon wind velocity (1.7 m s^{-1}).

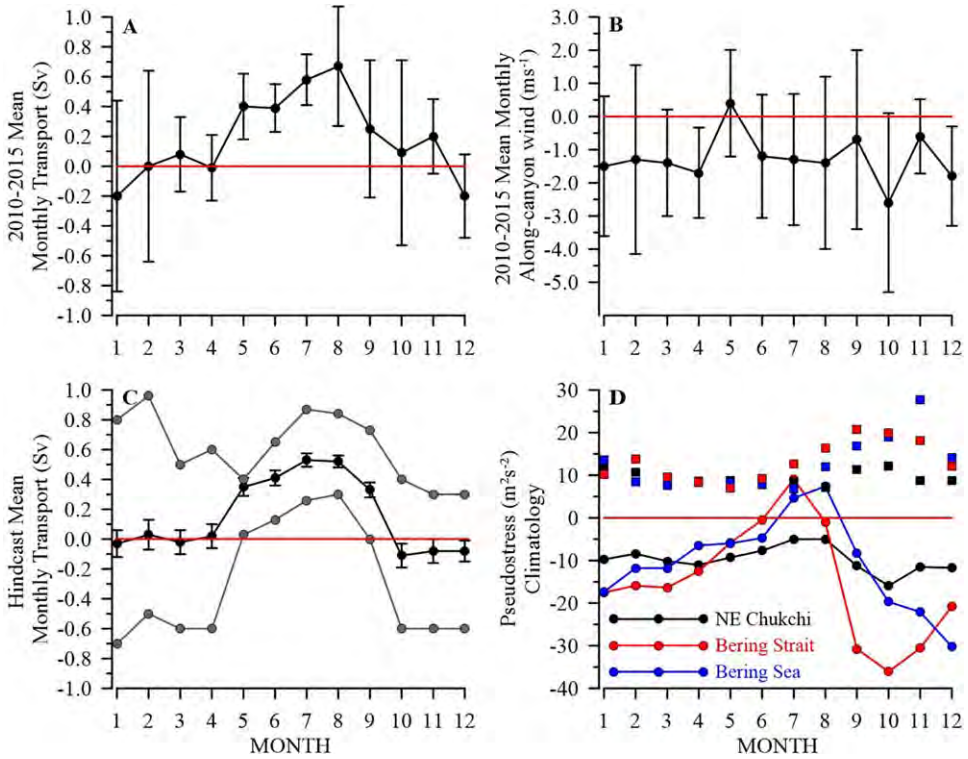

Figure 6. (a and b) The means (filled circles) and standard deviations (error bars) on the monthly transport and along-canyon wind velocity, respectively, for the 2010–2015 period. (c) The mean monthly transport (black line and circles) and 95% confidence limits (error bars) based on the January 1979 to July 2015 GLM hindcast. The gray lines and circles indicate the maximum and minimum values in each month. (d) Displays the monthly means (circles) and standard deviations (squares) of the pseudostress for the January 1979 to July 2015 period at the three locations used in the GLM.

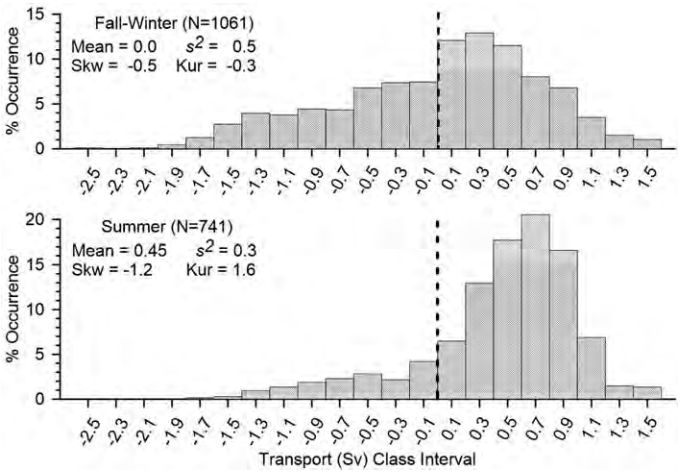

Figure 7. Probability density functions of the mean daily transport in Barrow Canyon for (October–April; top) winter and (May–September; bottom) summer. Each plot includes the value of the mean, sample variance (s^2), and the skewness (Skw) and kurtosis (Kur) coefficients, computed per *King and Julstrom* [1982]. The vertical dashed line delineates the upcanyon from the downcanyon class intervals.

upcanyon. Skewness is more negative in summer than in fall/winter even though upcanyon flows are more frequent and stronger in fall and winter (i.e., 21% of all fall/winter transports are ≤ -0.6 Sv, but only ~7% of summer upcanyon transports are ≤ -0.6 Sv). The seasonal skewness differences reflect seasonal changes in the kurtosis. The summer pdfs have positive kurtosis; ~76% of all mean daily transports are clumped within 1 SD of the mean. The fall/winter (and record length) pdfs have negative kurtosis, implying that upcanyon flow events are very intermittent and more frequent and larger than those of summer. Both pdfs fail the Kolmogorov-Smirnov goodness of fit test for normality at the 95% confidence level.

Variability in the along-canyon transport is largely wind-forced (Figure 4). The maximum correlation accounts for ~47% of the transport variance, using the wind-component projected along 67°T and leading the transport by ~1 day. This result is similar to that found by *Itoh et al.* [2013] at the mouth of the canyon and by *Gong and Pickart* [2015] from an assemblage of synoptic cross-canyon velocity sections. The lagged response of the transport may reflect the spin-up time (h/r) for the bottom boundary layer; where h is the water depth (~45 m) and r the linear resistance coefficient. For a frictional time scale of 1 day, r is $\sim 5 \times 10^{-4}$ m s^{-1}, consistent with estimates from other continental shelves [*Brink*, 1998].

Although the local winds explain nearly half the transport variance, there are prominent deviations from this relationship. For example, there is a distinct annual transport cycle (Figure 6a), but the mean monthly along-canyon winds for the 2011–2015 period showed no seasonality (Figure 6b). Moreover, from June to August 2011, the mean flow was ~0.5 Sv downcanyon while the winds averaged ~3 m s^{-1} upcanyon (Figure 5). In contrast, the average transport was upcanyon at 0.5 Sv from November 2012 to March 2013 when the mean winds were upcanyon at ~4 m s^{-1}. Such large transport differences cannot be ascribed to the small changes in local winds.

One clue to the differential transport responses to the winds is apparent in comparing the regional wind and sea level pressure maps for June, July, August, and September 2011 (Figures 8a–8d), December 2012, and January, February, and March 2013 (Figures 8e–8h). From June to September 2011, winds over the northeastern Chukchi shelf were easterly or northeasterly at 3–6 m s^{-1}. In all months except September, the flow was downcanyon at rates of 0.2–0.7 Sv. Only in September did the flow become upcanyon, coincident with the onset of strong northeasterly winds over the northeastern Chukchi shelf *and* northerly winds over the northern Bering Sea. The transport was upcanyon at ~−0.2 Sv in December 2012 when the along-canyon winds were northeasterly at ~2 m s^{-1}, but the winds over the northern Bering shelf were northerly at 5–7 m s^{-1}. Upcanyon transports of ~−1 Sv occurred in January and February 2013 as well, when strong northeasterly (northerly) winds of 4–6 m s^{-1} blew over the northeastern Chukchi (Bering Strait). The mean transport was nil in March when winds over the northern Bering Sea collapsed, although moderate northeasterly winds of 3–4 m s^{-1} persisted over the northeastern Chukchi. These results recall those of *Danielson et al.* [2014], who showed that circulation variability in the eastern Chukchi Sea was mediated by northward propagating, downwelling and/or upwelling, long, continental shelf waves generated on the Bering Sea shelf. In addition, other adjustments in the shelf wide pressure field arise from coastal convergences and divergences over the entire Chukchi [*Winsor and Chapman*, 2004; *Spall*, 2007] and northern Bering shelves [*Danielson et al.*, 2014].

3.3. Transport: Hindcast and Climatology

Based on the preceding results and following *Danielson et al.* [2014], we applied general linearized models (GLM) in an effort to improve transport predictability in Barrow Canyon. This approach recognizes that it is

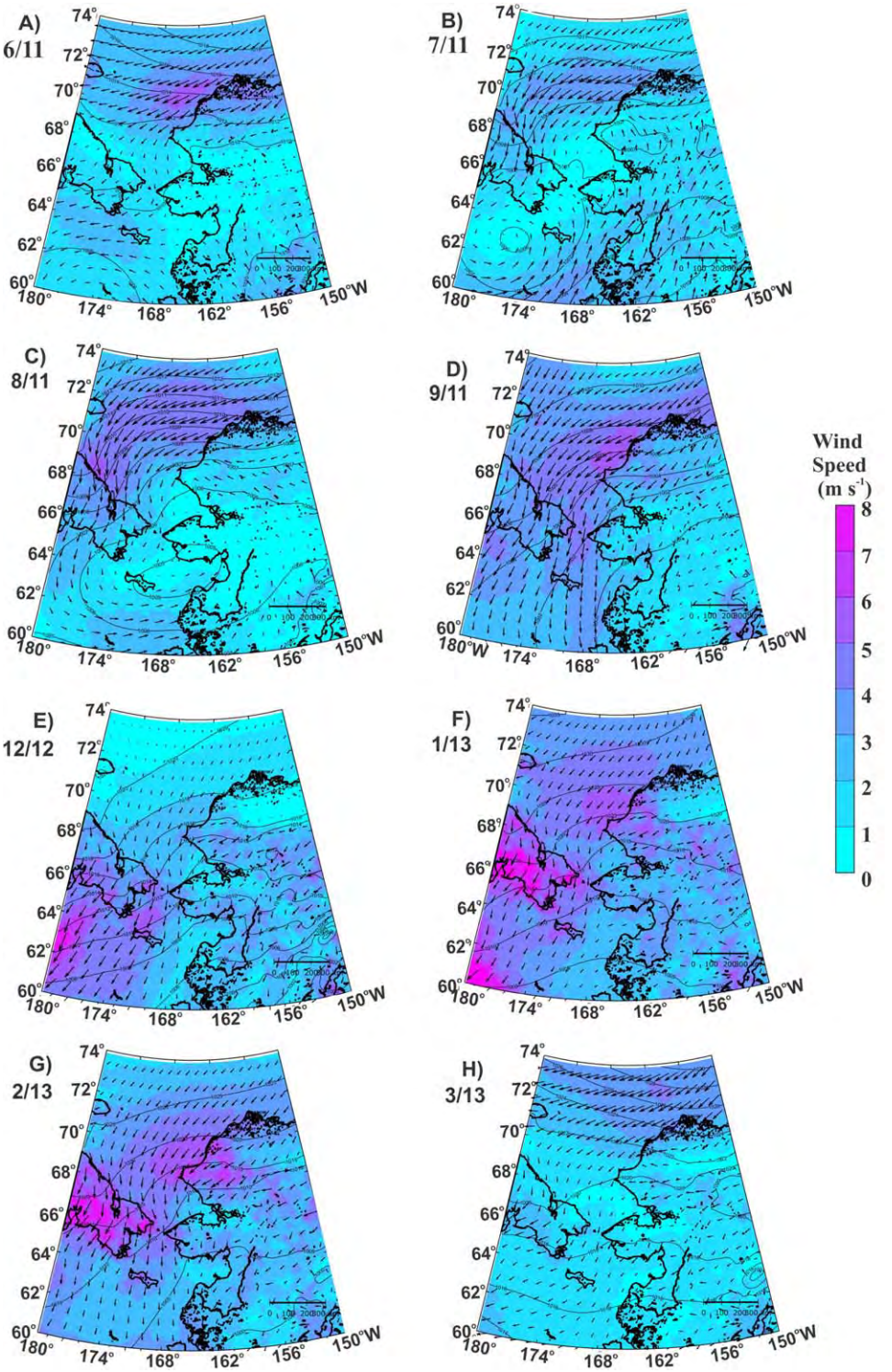

Figure 8. Mean monthly maps of sea level pressure (contours), wind speed (color), and direction (arrows) over the northern Bering and Chukchi seas. The 2011 maps are for: (a) June, (b) July, (c) August, and (d) September and the 2012–2013 maps are for: (e) December, (f) January, (g) February, and (h) March.

the alongshore integral of the shelf winds upstream of the point of interest that affects the local circulation [e.g., *Gill and Schumann*, 1974]. Our GLM uses NARR winds at locations listed in Table 1 in Barrow Canyon (BC2), Bering Strait (A3), and the northern Bering Sea shelf (C40). We proceeded by first finding the highest

correlation for both the rotation angle and time lag by regressing the transport against each of the six individual wind components over the entire transport record and then applying these lags and angles to the GLM regression (and given in Table 2). Separate regressions were made for summer (May–September) and fall/winter (October–April).

The summer and fall/winter regressions (rows 2 and 3 of Table 2) explain 55% and 59%, respectively, of the transport variance. Although these seasonal differences are not substantially different from one another, the GLM results are a significant improvement over models using only Barrow Canyon winds by explaining ~10% or more of the variance. All but the C40 (Bering shelf) model coefficients differ significantly from their seasonal counterparts. For example, the summer intercept is almost 30% larger than the winter intercept, and both seasons' intercepts are positive and consistent with downcanyon transport being maintained by an alongshore pressure gradient in the absence of wind forcing. In contrast, the magnitudes of all the winter wind coefficients (except C40) are significantly larger than the summer coefficients.

We applied the GLM to hindcast mean daily Barrow Canyon transports using NARR winds from January 1979 to July 2015 and then formed monthly means to construct a climatological annual transport cycle (along with 95% confidence limits and the range in mean monthly transports, Figure 6c). The climatology suggests that three seasons comprise the annual transport cycle: (1) winter (January–April), when the net transport is zero; (2) summer (May–September), when the net transport is ~0.45 Sv downcanyon; and (3) fall (October–December), when the net transport is ~−0.1 Sv upcanyon. The ranges for summer months imply that individual monthly transports are always downcanyon, whereas the fall/winter ranges indicate that individual monthly transports can be upcanyon or downcanyon. The hindcast cycle is similar in phasing to the annual cycle computed from the 5 years of measurements (Figure 6a), and the 95% confidence limits on the observed monthly means overlap those of the hindcast values.

As a further illustration of the seasonality in wind forcing over the Bering and Chukchi seas, we show the seasonal variation in the alongshore pseudostress (the product of wind speed and the alongshore wind component and which avoids uncertainties in choosing ice-ocean drag coefficients) from the northern Bering Sea, Bering Strait, and Barrow Canyon derived from the 37 year NARR record (Figure 6d). Although the annual pseudostress cycles at each location are nearly in-phase everywhere, the annual amplitudes of the pseudostress at the Bering locations are ~30–45 $m^2\ s^{-2}$ while that for Barrow Canyon is ~5 $m^2\ s^{-2}$. The monthly standard deviations are nearly equal at all locations from December to July, and over Barrow Canyon they are virtually constant throughout the whole year. At the Bering locations pseudostress variability from September to November is 2–3 times greater in comparison to other months and/or to Barrow Canyon. These differences suggest that the influence of remote winds on Barrow Canyon transports should vary considerably from year-to-year, especially in autumn.

Variability in the entire monthly hindcast record (not shown) is dominated by the annual signal, which oscillates about a long-term mean value of 0.16 Sv. Monthly transport anomalies derived from the hindcast climatology cycle (Figure 9) show that the anomaly magnitudes are large and exceed 0.2 Sv in about one-third of the months. Fall and winter anomaly magnitudes are ~0.2 Sv on average, twice those of summer. The maximum mean monthly transport is ~1.0 Sv (February 1989), and the minimum is ~−0.7 Sv (January 2001). Month-to-month changes in anomaly sign show little persistence, although upon smoothing with a 13 month running mean, there is a suggestion of anomaly magnitudes of ~0.1 Sv persisting for 3–10 years. For example, transports between 1979–1988 and 1999–2006 were ~0.1 Sv below the long-term average, while those from 1989 to 1998 and since 2006 were above the mean by a similar amount.

As discussed later, monthly transports that are either upcanyon or downcanyon in fall or winter likely have a profound influence on the circulation and water masses on the northeastern Chukchi Sea. We thus consider the larger-scale atmospheric patterns associated with monthly transport anomalies. Figure 10 shows maps of atmospheric pressures and surface winds composited using all March and October months (representative of the winter and fall, respectively) for which the transport anomalies exceed one standard deviation from the climatological monthly mean. The maps in the top row indicate that abnormally large winter and fall upcanyon transports are associated with a deep Aleutian Low, centered along 52°N between 150°W and 170°W, and a strong Beaufort High. The juxtaposition of these pressure systems impels northeasterly (northerly) winds over the Chukchi (Bering) shelves. For months when the downcanyon transport is anomalously large, winds are feeble, the Aleutian Low is weak and displaced into the Gulf of Alaska, and the meridional pressure gradients over northern Alaska are diminished.

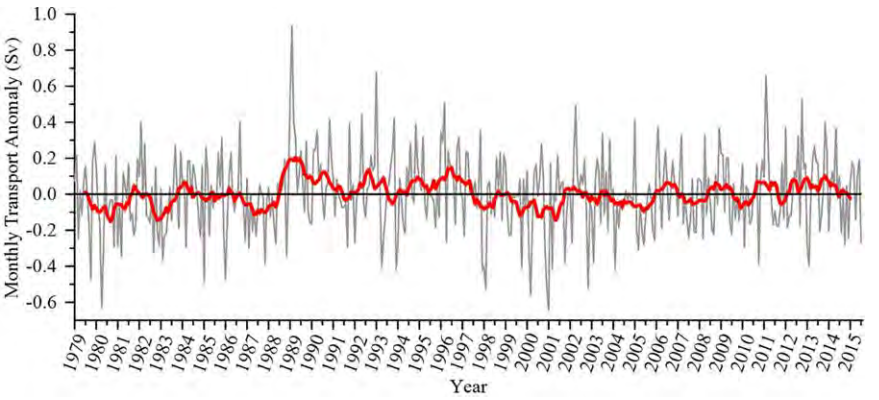

Figure 9. Monthly transport anomalies (gray) for the 1979–2015 period based on the GLM hindcast. The thick red curve is the 13 month running mean of the anomalies.

The observed transport pdfs indicated large seasonal differences in the kurtosis, which we further explore using the mean daily hindcast transports to compute cumulative probabilities of flow event duration and the total number of events for each season for both the upcanyon and downcanyon cases (Figures 11a and 11b, respectively). (Transport events that extend across seasons were assigned to the season in which most of the event occurred.)

From the climatological perspective, there are nearly equal probabilities of upcanyon and downcanyon events within any given season. Consequently, seasonal differences in kurtosis are associated with seasonal

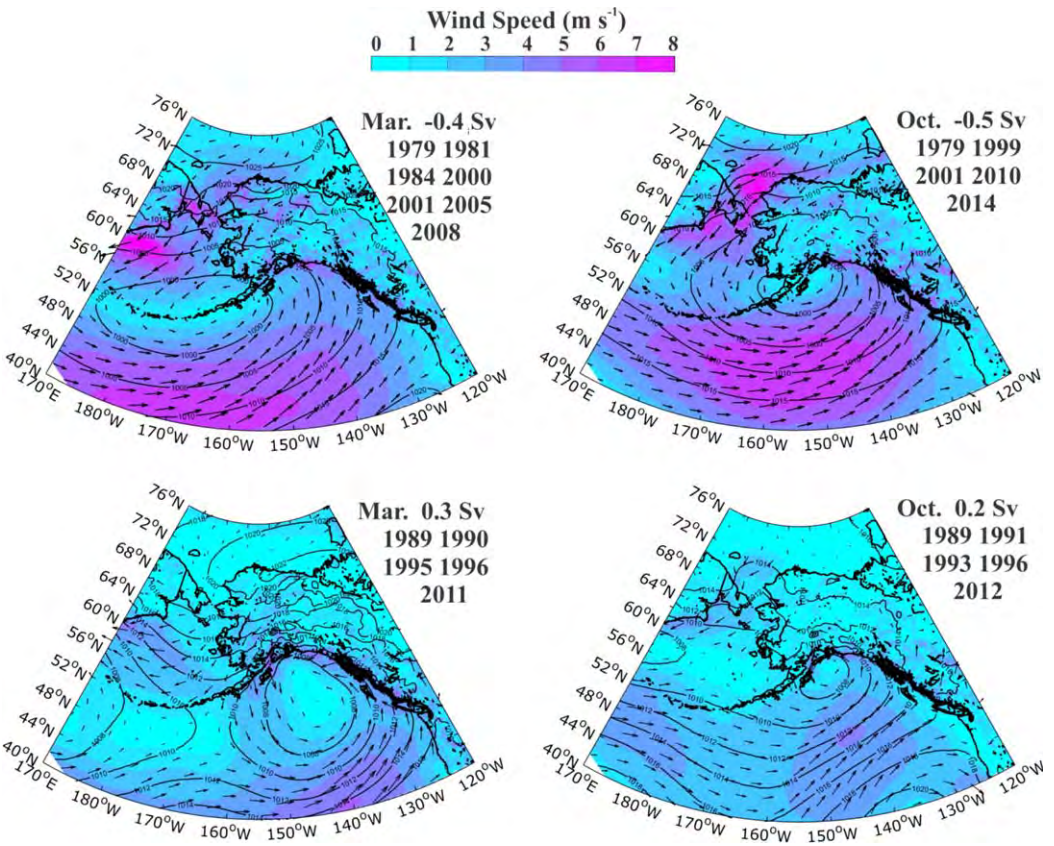

Figure 10. Sea level pressure (contours), surface wind vectors (arrows) and wind speeds (colors) for (left) March and (right) October in which there was anomalously large upcanyon (top row; ci = 5 mb) and downcanyon transports (bottom row; ci = 2 mb). The maps are composites based on the month and years shown to the right of each map, which includes the mean monthly transport for those years.

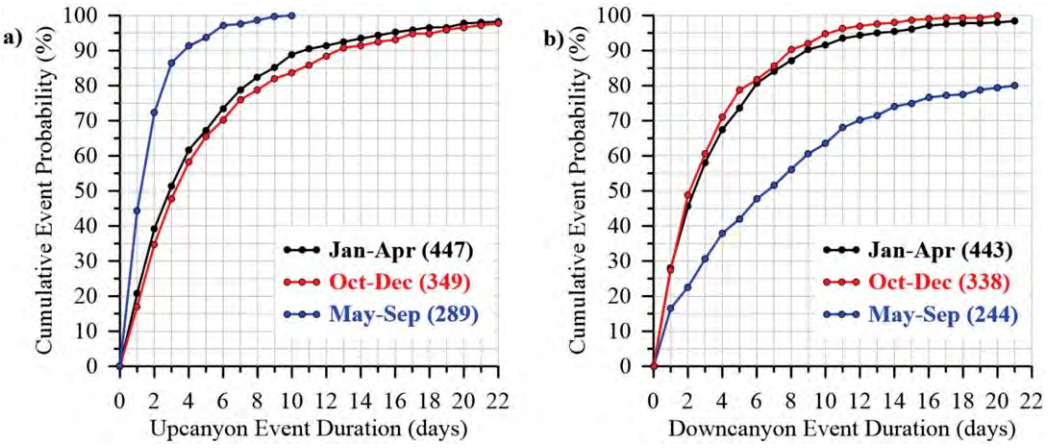

Figure 11. The seasonal cumulative probabilities for (a) upcanyon and (b) downcanyon events based on the hindcast transport record. The numbers associated with the seasons in the legend on each graph refer to the number of events over the 37 year record.

differences in event durations and/or transport magnitudes. Differences in event durations are most striking in summer, when 75% of upcanyon events are $\leq$2 days, and only 10% are 4–10 days in length (with 10 days being the maximum length). By contrast, only $\sim$20% of summer downcanyon events are $\leq$2 days duration, and more than 40% exceed 10 days (with the maximum duration being 120 days). Short ($\leq$2 days) duration events have smaller mean daily transport magnitudes than events $>$2 days. Hence, in summer, the magnitude of the mean daily downcanyon transport is $\sim$2.5 times larger than that for the upcanyon transport. Differences in event durations are smaller in fall and winter, when $\sim$75% of upcanyon and downcanyon event durations are $\leq$5–6 days, and mean daily transport magnitudes for each event are more equal.

3.4. Thermohaline Variability

Our description of temperature and salinity variations at the head of the canyon is based on near-bottom measurements (within $\sim$4 m of the seabed). Although these may not be representative of the water column, they provide a sense of the spatial and temporal scales in water mass variability. We first address these scales by examining the potential temperature (θ) and salinity (S) records from moorings BC1, BC2, and BC5 for the August 2010–August 2012 period (Figure 12; we omit the other records to enhance clarity). BC5 data are representative of θ and S at BC4 and BC6. The BC3 θ and S records are similar to those at BC1 and BC2, but the magnitude of the variations at BC3 is smaller.

There is little seasonal variability in salinity at BC5 where the average and standard deviation of $S = 32.6 \pm 0.3$. BC5 temperatures are $\theta = -1.4 \pm 0.7$°C, with θ near-freezing in all months except between June and November. In contrast, BC1 and BC2 have distinct seasonal variations. From late November/early December through April/early May, θ is at or near the freezing point, and the salinity average and standard deviation are $\sim$33 and 0.5, respectively. Consequently, the density of near-bottom waters in winter decreases moving offshore. At all locations, but most noticeably at BC1 and BC2, there are episodes of warm (-1.5 C$< \theta <\sim$0 C), salty ($\geq$33.1) intrusions in fall and winter, which are associated with upcanyon flows of slope waters (discussed later). There were also periods when very salty ($>\sim$33), near-freezing waters were present at BC1 and BC2 (and BC3) but not at BC5, e.g., February–March 2011 and January–February 2012. In fact, the saltiest fractions occur more frequently at BC1 than at BC2, in spite of BC1 measuring at a shallower depth. These are cold, salty, recently formed winter waters, most likely produced in the latent heat polynyas along Alaska's northwestern coast [*Cavalieri and Martin*, 1995]. They are subsequently transported into the head of the canyon [*Weingartner et al.*, 1998] where, as expected, they are trapped to the coast by the sloping topography [*Chapman*, 2001].

The cross-shore density gradient reverses sign from June to September, when, in general, salinity (and density) increases and temperature decreases moving offshore. This reversal has little to do with changes in water properties at BC5 but is instead due to the impressive changes in temperature and salinity at BC1 and BC2. Warming and freshening begins in May and proceeds gradually via a series of pulses coincident with energetic downcanyon transport events. In 2012 (and perhaps 2010), these pulses gave way to a sustained

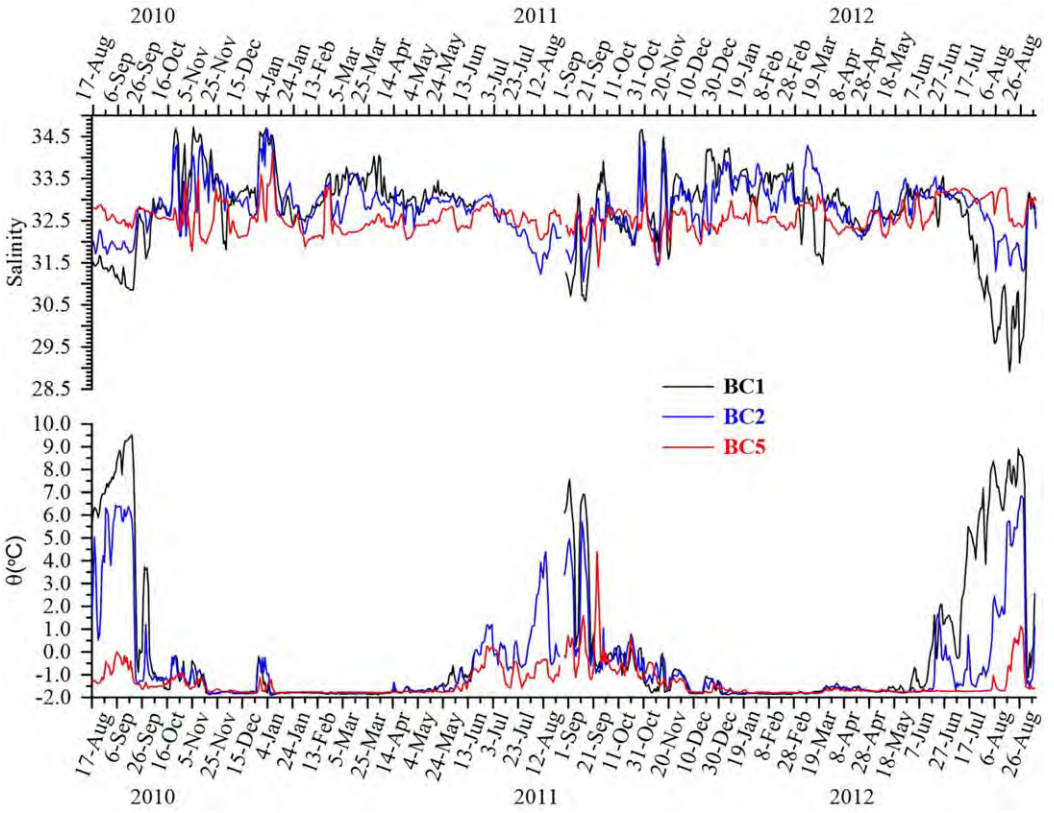

Figure 12. (top) Time series of salinity and (bottom) potential temperature θ, at moorings BC1 (black), BC2 (blue), and BC5 (red) for the August 2010–August 2012 period.

period of warm (8°C), fresh (29–30) ACW, which persisted at BC1 through August and September. The salinity records imply that the cross-shore salinity gradients within the canyon attain their maximum values in these months. In August and September 2010, the mean density difference between BC1 and BC3 was ∼1.4 kg m^{-3} implying a vertical shear in the along-canyon velocity of $\sim 5 \times 10^{-3}$ s^{-1}, assuming thermal wind balance and that the gradient holds over the entire water column. Under these assumptions, the velocity difference over the uppermost 30 m of the water column between BC1 and BC3 would be ∼20 cm s^{-1}. If we further assume that this shear was typical for August and September 2010, the baroclinic geostrophic contribution to the total along-canyon transport was ∼0.15 Sv, which is in line with the synoptic observations of *Münchow and Carmack* [1997], *Pickart et al.* [2005], *Gong and Pickart* [2015], and the model results of *Signorini et al.* [1997]. By comparison, the measured transport for this period was ∼0.8 Sv, suggesting the barotropic component accounted for ∼80% of the canyon transport.

Figure 13 shows the 5 year BC2 temperature and salinity time series along with the mean daily transport. Clearly the inferences drawn from the 2 years shown in Figure 12 regarding the seasonal variability in temperature and salinity at BC2 hold over the entire record. The longer record underscores the tremendous interannual variability in water mass properties. For example, the maximum water temperature in summer and fall 2013 was ∼3–4°C cooler than in the other years, and while winter bottom temperatures were always close to the freezing point, winter-to-winter variations were primarily associated with upcanyon incursions of warmer slope waters. There is also variability in the timing of the spring and/or summer arrival of above-freezing temperatures. We assessed this by examining the dates when BC2 temperatures first reached 0°C and 2°C. (The arrival of water of −1°C is followed within a few days by water at 0°C, and the 1.5°C and 2°C arrival dates are similarly close). The "early" summers of 2011, 2012, and 2015 all detected 0°C between the 20th and 22nd of June, with temperatures rising quite rapidly afterward. In 2011 and 2012, 2°C water occurred during the first week of August, and in 2015 it arrived a full month earlier. In the "late" summers of 2013 and 2014, 0°C water appeared on the 29th and 18th of July, respectively. In 2013, temperatures

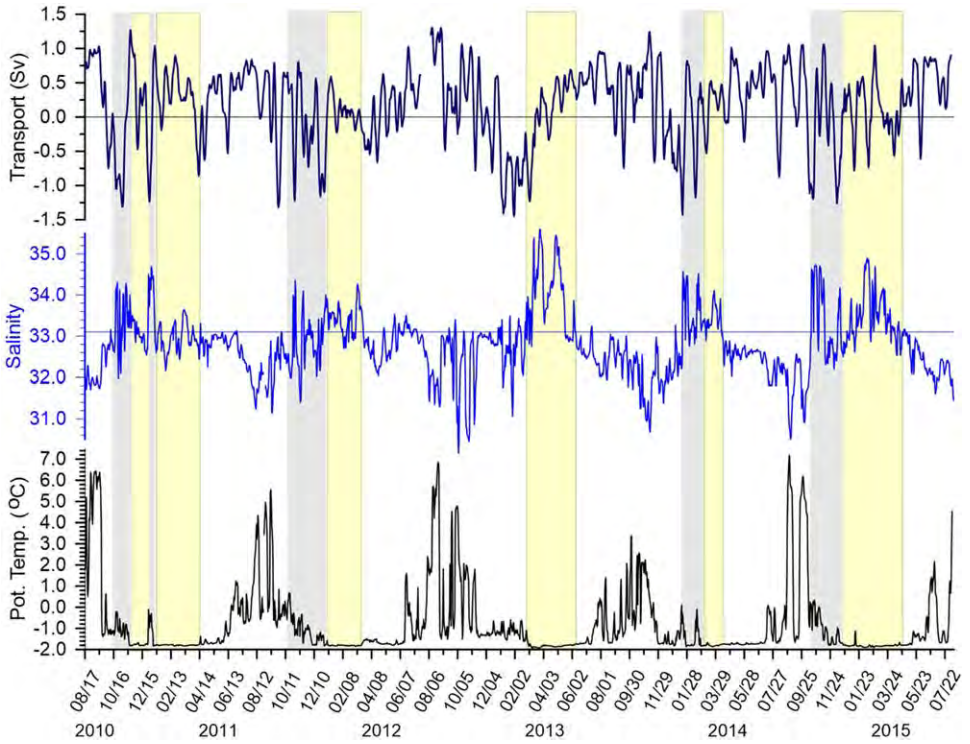

Figure 13. (bottom) Time series of temperature and (middle) salinity from mooring BC2, and the along-canyon transport (smoothed with a 7 day running mean; top). The horizontal line on the salinity plot delineates the 33.1 value. The light gray shading encompasses the periods of upcanyon transports that contained lower halocline and Atlantic Water signatures (e.g., salinity>33.1 and > -1.6°C). The light yellow shading captures periods of dense water ($S > 33.1$ and θ = freezing point).

reached 2°C in late September, and in 2014 this benchmark occurred in late August. Variations in the spring/summer arrival of warm bottom waters are not obviously related to the spring or early summer transports. The average transports from April to June in the "late" summers of 2013 and 2014 were ~0.38 Sv and more than double the corresponding averages for the "early" summers. Nor did we find a compelling relationship between the May and June ice extent over the Chukchi Sea shelf and the timing of warm water arrival. Such a relationship would suggest that solar penetration and heating of subsurface waters was responsible for the difference in arrival times. The lack of convincing connections between the timing of the summer arrival of "warm" water and summer transport magnitudes or ice extent suggest that the summer warm water signature is established by conditions well south of Barrow Canyon and most likely on the Bering Sea shelf.

The fresh, warm waters of late summer/fall routinely terminate with the upcanyon transport of salty (>33.1) water with θ between -1.6°C and 0.5°C. Waters with these characteristics are found over the continental slope within the lower halocline (140–180 m depth) and/or even deeper (~200 m) within the Atlantic Layer [*Shimada et al.*, 2005]. The gray-shaded regions in Figure 13 highlight the more prominent packets of upcanyon events, in which lower halocline or Atlantic Water was transported to the head of the canyon. Most of these (indeed four of the five highlighted events) occur in the October–December period. Following these events, temperatures at the head of the canyon decreased to ≤ -1°C.

Interestingly, the depth of the slope water source (based on the θ/S characteristics described earlier) does not appear to be a function of the magnitude or duration of the upcanyon flow events as suggested by *Signorini et al.* [1997]. The most obvious example of this was the prolonged and strong upcanyon flows that occurred between December 2012 and February 2013. Throughout this time the upcanyon transport had salinities <33.1 and $\theta \leq -1$°C. In contrast, the warmest ($\theta \sim -1$°C) and most saline (~34.5) waters occurred during the sequence of upcanyon and downcanyon flows of October 2014. Hence, the magnitude and persistence of upcanyon flow events do not solely determine the source depth of slope waters fluxed into the canyon. Other mechanisms, likely occurring over the shelfbreak and slope, must be important in this regard.

4. Discussion

4.1. Transport Comparisons

Our average transport estimate of ~0.2 Sv at the head of Barrow Canyon is in reasonable agreement with the modeled mean transport of *Spall* [2007] of ~0.25 Sv, but it is ~50% smaller than the ~0.45 Sv average of *Itoh et al*. [2013] determined at the mouth of the canyon. We examine the possibility that these differences are a result of sampling bias and/or unaccounted transports into the canyon between its head and mouth. We first address these possibilities using vertically averaged means and variances from various moorings located in Barrow Canyon and over the northeastern shelf for the 2010–2011, 2011–2012, and 2012–2013 periods shown in Figures 14a–14c, respectively. (The plot contains two different scales for the currents; scales within the blue box are one-half those outside of the box to enhance viewing the smaller currents farther from the canyon axis.)

Our array may be biased if there is substantial flow moving northeastward between the offshore end of the BC mooring array and the southeast side of Hanna Shoal. This undetected flow would enter the canyon north of the BC array. We examine this possibility using results from moorings A, B, and C (Figure 14b) that extend northwestward from the end of the BC array to the southern side of Hanna Shoal. The means and standard deviations of these records were ~2 cm s^{-1} and ~10 cm s^{-1}, respectively. The vectors and the ellipses are oriented toward the head of Barrow Canyon (similar to the statistics from moorings BC4 and BC5) at A and C, although the flow direction at B suggests that some of this flow might enter the canyon north of the BC array.

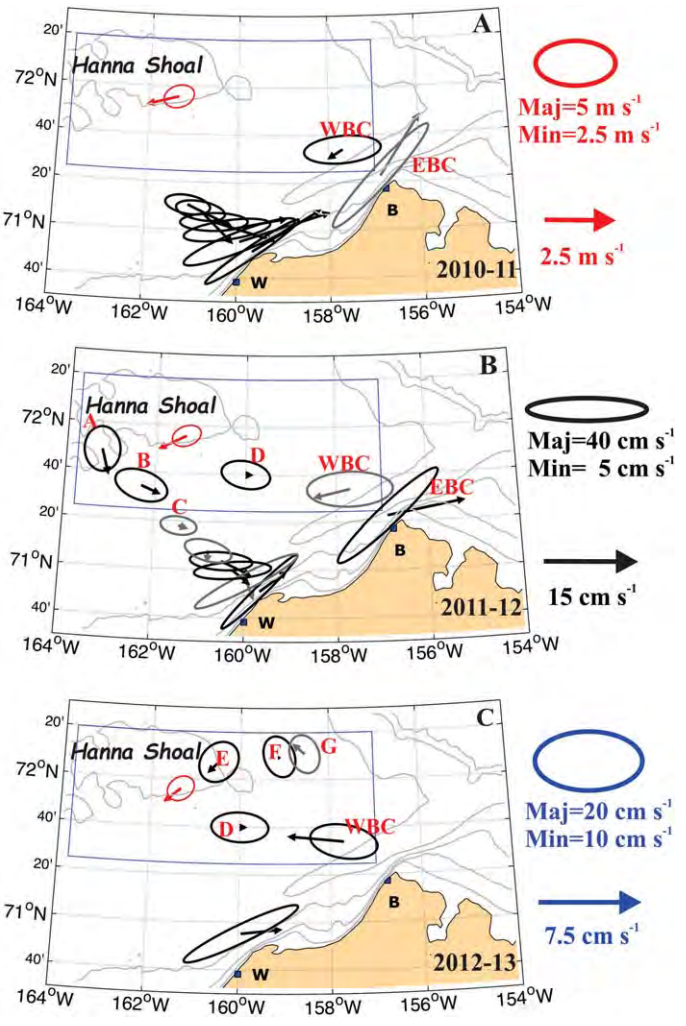

Figure 14. Vertically averaged mean velocity vectors and variance ellipses for currents and winds in (a) 2010–2011, (b) 2011–2012, and (c) 2012–2013. Red symbols and text are for winds, black are for currents outside of the blue box, and blue are for currents within the blue boxes. Gray (black) vectors and ellipses in each figure denote record lengths of from 6 to 10 (11 to 12) months duration.

At each mooring, the mean flow along the minor axis was <1 cm s^{-1} southwestward but not significantly different from zero at the 95% confidence level. This finding is consistent with that of *Pickart et al*. [2016], who observed southeastward flow along the south side of Hanna Shoal from synoptic summer velocity and hydrographic sections. Collectively these results suggest that: (1) flow over the northeastern Chukchi Sea shelf south of Hanna Shoal was funneled toward the head of the canyon (consistent with inferences by *Weingartner et al*. [2005]) and (2) that there was little northeastward transport from the central Chukchi to the shelf between Hanna Shoal and Barrow Canyon. Both findings comport with the model results of *Winsor and Chapman* [2004] and *Spall* [2007].

We next examine current data for the shelf east and northeast of Hanna Shoal. At mooring D (Figures 14b and 14c), the mean vertically averaged flow was not statistically different

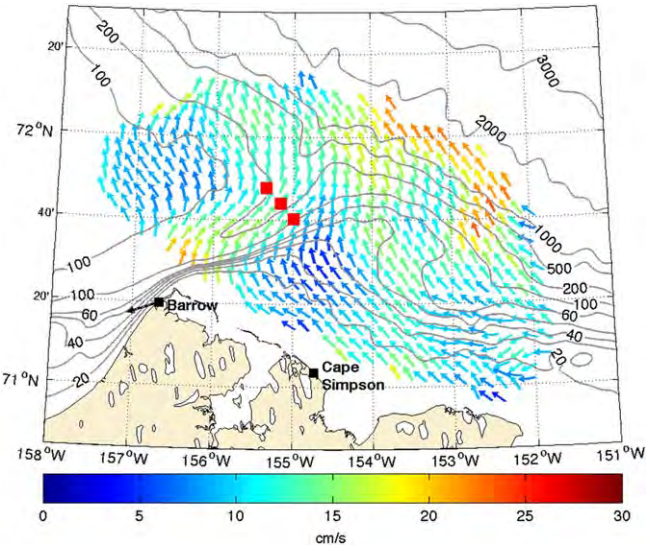

Figure 15. Mean September–October 2013 surface current map of the western Beaufort Sea shelf and the northern end of Barrow Canyon. The mean winds at Barrow were from the east-northeast (as indicated by the arrow) at 3 m s^{-1}. The red squares at the mouth of Barrow Canyon are the locations of the moorings discussed by *Itoh et al.* [2013].

from zero. There appears to be negligible flow overly the weakly sloping shelf between the 40 and 55 m isobaths as measured by moorings E, F, and G northeast of the Shoal in both 2012–2013 (Figure 14c) and in 2013–2014 (not shown). Although somewhat ambiguous, these results suggest that this portion of the shelf is not a major feed for Barrow Canyon. There is the possibility, however, of net eastward transport between the 55 m isobath and the shelfbreak.

A second potential source of bias is in the mooring array at the mouth of the canyon. Recall that *Itoh et al.*'s [2013] transport estimates derive from three moorings, deployed at 10 km intervals, from east to west, on the 80, 250, and 150 m isobaths, respectively (Figure 15). The gap between their westernmost mooring and the 70 m isobath on the west side of the canyon is ~30 km (~5 times the baroclinic radius of deformation). This gap is wide enough to permit the ~15 km wide, subsurface, eastward flowing Chukchi shelfbreak current carrying winter waters [*Corlett and Pickart*, 2017] to enter the western side of the canyon. (Their estimate is tentative insofar as it is based on a compilation of synoptic sections collected between the months of May and October in different years.) We expect that the eastward shelfbreak flow follows the isobaths around the western lip of Barrow Canyon and continues upcanyon along the western wall. Proceeding upcanyon, this transport should diminish as it becomes entrained into the prevailing downcanyon flow along the eastern wall. This additional mass transport would be captured by the mooring array at the mouth of the canyon, but not the array at the head of the canyon. This interpretation is reflected in *Shroyer*'s [2012] synoptic sections and in the vertically averaged current statistics from two moorings deployed west of Barrow on the 70 m isobath on the eastern (EBC) and western (WBC) sides of the canyon (Figures 14a–14c). In all 3 years, the vertically averaged flow at WBC was statistically significant and southwestward (or westward in 2012–2013) at ~1–3 cm s^{-1}. By contrast, along the eastern wall of the canyon the mean flow was ~15 cm s^{-1} northeastward and statistically significant.

Another potential mass source is associated with westward flow over the Beaufort shelf. As seen in Figure 15, the HFR-averaged surface currents for September–October 2013 between the coast and the 40 m isobath (~50 km offshore) were ~7 cm s^{-1}. If this estimate is comparable to the vertically and annually averaged currents, then the western Beaufort shelf contributes ~0.07 Sv into Barrow Canyon upstream of the canyon mouth. The mean winds on the Beaufort Sea shelf are westward year-round suggesting that this shelf transports water into the canyon.

Taken together the subsurface eastward flow along the Chukchi shelfbreak and the westward flow from the Beaufort shelf may add ~0.15 Sv to the ~0.2 Sv canyon outflow we measured. If correct, these contributions substantially reduce the 0.25 Sv transport deficit between the head and the mouth of the canyon. We emphasize, however, that the estimates of the additional mass sources are tentative at best and await better resolution.

4.2. Consequences of Transport Seasonality

When compared to the transport climatology in Bering Strait [*Woodgate et al.*, 2005b], we find that, on average in summer, ~40% of the Bering Strait summer transport is carried into the head of Barrow Canyon, but none of the Strait's transport enters the canyon in fall and winter. This finding implies fall/winter flow convergence over the shelf south of Barrow Canyon because the net northward Strait transport must be

diverted elsewhere, with the Central Channel, Herald Valley, and Long Strait being the likely avenues of egress. Although diversion has been inferred to happen in some winters [e.g., *Weingartner et al*., 1998] and in numerical models subject to synoptic wind events [*Winsor and Chapman*, 2004; *Spall*, 2007], our results imply that it is an annual occurrence. If so, seasonal switching of the points of entry into the Arctic Ocean of Pacific waters should affect the shelfbreak circulation structure and the seasonality of slope/basin exchange. We next consider other implications of this annual cycle.

4.3. Hydrographic Implications

The downcanyon advection of warm waters characteristic of summer effectively concludes with the upcanyon transport of colder waters in fall. The duration and intensity of these upcanyon flows may be critical in initiating freezeup on the northeastern Chukchi shelf because the oceanic heat flux convergences associated with these events can be substantially greater than the heat loss to the atmosphere [*Weingartner et al*., 2013a]. The interplay between upcanyon and downcanyon transports in fall may also affect the properties of dense winter waters produced on the shelf. Large volumes of dense water can be produced in the extensive latent heat polynyas along the northwest coast of Alaska, which are most prominent in December and January [*Cavalieri and Martin*, 1995; *Weingartner et al*., 1998; *Ladd et al*., 2016]. The initial polynya salinity depends upon advection from either the south (low to moderately saline Bering waters) or from the north (MW and WW) and is a key ingredient in establishing the properties of the dense water formed [*Winsor and Chapman*, 2002]. Winter circulation can also affect dense water production. If the along-shelf flow collapses, dense water residence time in the polynyas can be prolonged and thus become denser over the duration of the polynya event. In addition, the absence of an along-shelf flow implies that a greater fraction of the dense water is carried cross-shelf by eddies [*Gawarkiewicz and Chapman*, 1995] rather than into the canyon by the along-shelf flow. Finally, negligible winter canyon transport implies sluggish flow over the northeastern Chukchi shelf, thus expanding the time for exchanges between the seabed and bottom waters. Each of these processes affects the properties of the dense winter water that ultimately enters the Arctic Ocean.

4.4. Shelf Response to Wind Forcing

Transport variations are largely controlled by local and remote winds. The latter includes Bering Sea shelf winds, where the seasonal variations in wind stress are much larger than over the northeastern Chukchi Sea. The summer and fall/winter wind-transport regression coefficients were significantly different from each other with the summer intercept being ~30% greater than the winter intercept. One reason for this difference might be due to the baroclinic contribution to the downcanyon transport, which amounted to ~20% of the total August and September transport. The baroclinic tendency should weaken through fall, and in winter it should either vanish entirely or reverse, as suggested by our observations.

Seasonal differences in regression coefficients may arise from oceanic processes that mediate vertical stress divergence in the alongshore momentum balance. *Chapman and Lentz* [2005] demonstrated that for stratified shelves the frictional stress exerted by the bottom boundary layer (bbl) is diminished compared to the unstratified case so that stratification enhances the alongshore transport forced by an alongshore pressure gradient. The response depends upon the magnitude of the slope Burger number ($Bu = \alpha N/f$, where N is the buoyancy frequency and α is the bottom slope). Bottom slopes are $\sim 5 \times 10^{-4}$ over the Bering and Chukchi shelves (and $\sim 10^{-3}$ in Barrow Canyon). N varies from $\sim 0.1\ s^{-1}$ in spring and early summer due to heavy stratification associated with ice melt [*Weingartner et al*., 2013b] and/or runoff over portions of the Bering Sea shelf [*Danielson et al*., 2012] to $\sim 0\ s^{-1}$ in winter [*Aagaard et al*., 1981, 1985]. As a result, Bu may be ≥ 0.2 in summer, and $Bu \sim 0$ in winter on the shelf. Complete bbl shutdown occurs for $Bu > 1$ [*Macready and Rhines*, 1993], but *Chapman and Lentz* [2005] find an appreciable increase in the alongshore transport for $Bu \geq 0.2$. Spatial variations in Bu render comparisons with theory difficult, but the seasonal differences in Bu are consistent with the summer intercept being larger than that of winter.

Chapman and Lentz's [2005] arguments imply that the summer wind coefficients should be greater than those of winter, but instead the winter coefficients are ~1.5 times greater than those of summer. Three possible reasons, operating alone or in concert, may account for this difference. First, fall and winter wind alongshore pseudostresses over the Bering Sea are greater than those of summer, and so the differences may simply reflect our choice of seasons in constructing the statistical model. Second, mobile sea ice covers all or portions of these shelves in fall and winter, and the ice-ocean drag should enhance the transfer of momentum from the atmosphere to the ocean [*Lu et al*., 2011; *Schulze and Pickart*, 2012]. Third, the winds

force rapidly propagating, long continental shelf waves in fall/winter when the stratification is weak. In summer, a greater fraction of the wave energy should be carried by smaller, more slowly propagating coastal-trapped waves. These are more susceptible to coastline scattering as they propagate northward, reducing the response of the transport to the winds.

4.5. Transport Intermittency

The intermittent nature of upcanyon and downcanyon transport events is an important feature of the flow. Intermittency is seasonally modulated, as reflected in the seasonal pdfs (Figure 7) and in the seasonal flow event duration pdfs (Figure 11). The differences, which arise because summer downcanyon (upcanyon) events are of greater (shorter) duration than those of fall and winter, may have consequences for shelf-basin exchange.

Upcanyon transport events have a maximum velocity scale of $\sim$0.4 m s^{-1} (Figure 3e), suggesting that the advective time scale for a parcel to travel from the mouth to the head of the canyon is $\sim$6 days. In summer, $\sim$5% of upcanyon flow events are $\geq$6 days, whereas in winter and fall, nearly 20% of upcanyon flows exceed 6 days. Thus, the transport of basin waters onto the shallower reaches of the Chukchi shelf is relatively rare and largely confined to fall and winter. Based on a comparison of the temperature and salinity records from moorings BC2 and EBC (where EBC is $\sim$110 km northeast of BC2, Figures 15a and 15b), we find that only $\sim$1/3 of the upcanyon events that transport slope waters as far as Barrow carry them to the head of the canyon.

Intermittency in downcanyon transports may have consequences on the formation of Arctic Ocean eddies. *Nof* [1991] argues that intermittent outflows can lead to unbalanced fluid patches that eventually break up into anticyclonic lenses. This mechanism is independent of the stability properties that evolve from quasi-geostrophic flows, such as that modeled by *Spall et al*. [2008] for a steady eastward shelfbreak current over the Chukchi/Beaufort slope. Presumably, short duration outflows from Barrow Canyon are more prone to generating eddies through imbalance, whereas longer, steadier duration outflows preferentially lead to quasi-geostrophic instabilities. Given the marked seasonal asymmetry in downcanyon event duration, Nof's arguments would suggest that current instabilities predominate in summer, and unbalanced motions prevail in fall and winter. Conceivably eddy generation sites might also change seasonally; unbalanced motions predominate at the canyon mouth while instabilities occur farther eastward along the Beaufort shelfbreak. As a final point, the halocline cold-core anticyclones generated along the Beaufort shelfbreak contain $\sim 5 \times 10^{10}$ m^3 Pacific-derived waters [based on a diameter of $\sim$20 km and a thickness of $\sim$150 m, *Zhao et al*., 2014]. A similar volume is transported during fall/winter downcanyon events of $\sim$2 days duration, which have a mean daily transport of $\sim$0.3 Sv. This agreement may be fortuitous but it suggests consideration be given to the connection between intermittency and basin eddies containing Pacific-derived waters.

As noted by *Itoh et al*. [2013], the summer downcanyon transport is a significant source of heat and freshwater to the Arctic basin by feeding the shelfbreak currents that flow eastward along the Beaufort shelfbreak and, within the upper ocean, westward along the Chukchi slope [*Corlett and Pickart*, 2017]. Upwelling and reversals from east to west of the Beaufort shelfbreak flow depend upon the magnitude of the easterly along-shelf winds [*Schulze and Pickart*, 2012], however, these winds may not cause a simultaneous reversal in the canyon transport. For example, in July 2011, strong northeasterly winds (Figure 8b) resulted in westward flow and upwelling along the entire Chukchi and Beaufort shelfbreak [*Spall et al*., 2014]. The Barrow Canyon transport in July 2011 was downcanyon (Figures 4 and 5), so the warm, fresh outflow was presumably carried westward along the Chukchi shelfbreak. Similarly, the mean westward surface flow (Figure 15) at the mouth of Barrow Canyon and over the Chukchi and Beaufort shelves and shelfbreaks was westward in September and October 2013 when mean winds were from the east-northeast at $\sim$3 m s^{-1} (Figure 14). These winds likely caused weak shelfbreak upwelling but not a complete reversal of the subsurface eastward shelfbreak jet [*Schulze and Pickart*, 2012]. However, the winds were not strong enough to reverse the transport at the mouth (Figure 15) or head of the canyon (Figure 5). *Schulze and Pickart* [2012] find that $>$65% of all westward wind events having wind speeds of 4–7 m s^{-1} result in significant Beaufort shelfbreak upwelling. Using the hindcast record we computed the probability of a downcanyon event versus easterly wind speed over the Beaufort slope (at the NARR grid point located at $\sim$72°N, 152°W). We find that $\sim$35% of all downcanyon transports occur under easterly winds when these wind speeds are within the 4–7 m s^{-1} range.

The confluence of the westward-flowing shelfbreak current and the downcanyon flow at the mouth of the canyon is presumably complicated. The PV structures of these flows differ; the shelfbreak flow has an upwelled frontal structure whereas the downcanyon flow is in the downwelled configuration. Upon converging at the mouth of the canyon, the different PV fields of both currents must adjust to one another. How this adjustment evolves remains to be determined but may involve intense mixing and a variety of submesoscale motions. In both the numerical model of *Watanabe* [2011] and *Nof*'s [1988] inviscid, analytical model the fate of the outflow is sensitive to the PV structure of both the outflow and the ambient current field. Interestingly, Nof finds that the outflow could be deflected to the east or to the west or even switch back and forth depending on PV structures.

5. Summary

We used a 5 year time series of transport, temperature, and salinity measurements obtained at the head of Barrow Canyon to describe the seasonality of these variables and to construct a 37 year hindcast of the mean daily transport. The annual cycle is in-phase with that in Bering Strait insofar as the maximum occurs in summer and the minimum in winter. The climatological Bering Strait transport is northward year-round [*Woodgate et al*., 2005b], but this is not the case in Barrow Canyon. Here the annual transport cycle consists of three seasons: (a) the May–September or "summer" season in which the transport is downcanyon (northeastward and into the Arctic Ocean) and averages 0.45 Sv, (b) the October–December or "fall" season in which the average transport is upcanyon (southwestward and onto the Chukchi Shelf) at 0.1 Sv and; (c) the January–April or "winter" season when the along-canyon transport is not significantly different from zero.

Acknowledgments

This work was supported by the Bureau of Ocean Energy Management (BOEM) grants M12AC000008 and M09AC15207. ConocoPhillips Alaska Inc. (CPAI), Shell Exploration and Production, Inc. (SEPI), and Statoil USA Exploration and Production supported the industry moorings south and east of Hanna Shoal as part of the Chukchi Sea Environmental Studies Program (CSESP). BOEM, CPAI, and SEPI collaborated in support of the 2010–2012 moorings at the head of the canyon. BOEM grant M11AC00007 supported the moorings northeast of Hanna Shoal. The EBC and WBC moorings in Barrow Canyon were supported by NSF grant PLR-1023446 with the data kindly provided by Stephen Okkonen. We thank David Leech for leading the mooring efforts and the officers and crews of the *Norseman II* for their efficient and safe operating efforts. The HFR systems were supported by BOEM, CPAI, SEPI, the Alaska Ocean Observing System (AOOS)/U.S. Integrated Ocean Observing System, and, at Cape Simpson, by the Alaska Coastal Impact Assistance Program. We thank the residents of Barrow, Pt. Lay, and Wainwright, the Ukpeaġvik Iñupiat Corporation and UIC Science for their assistance in the deployment of the HFRs. Special thanks to Warren Horowitz (BOEM), Caryn Rea and John Colloggi (CPAI), Michael Macrander (SEPI), Steinar Elroy (Statoil), and Molly McCammon (AOOS) for their program management efforts. Shenya Wisdom and Olgoonik Fairweather Inc. efficiently coordinated the field programs. NCEP Reanalysis data were obtained from the NOAA/OAR/ESRL PSD, Boulder, Colorado, USA, and available for downloading at the website: http://www.esrl.noaa.gov/psd/. The mooring and HFR data sets are archived with the authors and BOEM. In addition data for moorings WBC and EBC are at the Arctic Data Center: doi:10.18739/A21C7X and doi:10.18739/A20K5X. NODC accession numbers for the industry and BOEM mooring data are #0093399 and #0160090, respectively.

References

Aagaard, K., and A. Roach (1990), Arctic ocean-shelf exchange: Measurements in Barrow Canyon, *J. Geophys. Res.*, *95*, 18,163–18,175, doi: 10.1029/JC095iC10p18163.

Aagaard, K., L. K. Coachman, and E. E. Carmack (1981), On the halocline of the Arctic Ocean, *Deep Sea Res., Part A*, *28*, 529–545.

Aagaard, K., et al. (1985), Thermohaline circulation in the arctic mediterranean seas, *J. Geophys. Res.*, *90*, 4833–4846.

Allen, S. E., and X. Durrieu de Madron (2009), A review of the role of submarine canyons in deep-ocean exchange with the shelf, *Ocean Sci.*, *5*, 607–620.

Barrick, D. E., and B. J. Lipa (1986), Correcting for distorted antenna patterns in CODAR ocean surface measurements, *IEEE J. Oceanic Eng.*, *11*(2), 304–309.

Brink, K. H. (1998), Wind-driven currents over the continental shelf, *The Sea*, *10*, 3–20.

Cavalieri, D., and S. Martin (1995), The contribution of Alaska, Siberian, and Canadian coastal polynyas to the cold halocline of the Arctic Ocean, *J. Geophys. Res.*, *99*, 18,343–18,362.

Chapman, D. C. (2001), The influence of an alongshelf current on the formation and offshore transport of dense water from a coastal polynya, *J. Geophys. Res.*, *105*, 24,007–24,019.

Chapman, D. C., and S. J. Lentz (2005), Acceleration of a stratified current over a sloping bottom driven by an along-shore pressure gradient, *J. Phys. Oceanogr.*, *35*, 130–1317.

Coachman, L. K., K. Aagaard, and R. B. Tripp (1975), *Bering Strait: The Regional Physical Oceanography*, 172 pp., Univ. of Washington Press, Seattle, Wash.

Codispoti, L., C. Flagg, V. Kully, and J. H. Swift (2005), Hydrographic conditions during the 2002 SBI process experiments, *Deep Sea Res., Part II*, *52* (24–26), 3199–3226.

Corlett, W. B., and R. S. Pickart (2017), The Chukchi slope current, *Progr. in Oceanogr.*, doi:10.1016/j.pocean.2017.04.005, in press.

Danielson, S., E. Curchitser, K. Hedstrom, T. Weingartner, and P. Stabeno (2012), On ocean and sea ice modes of variability in the Bering Sea, *J. Geophys. Res.*, *116*, C12034, doi:10.1029/2011JC007389.

Danielson, S., T. Weingartner, K. Hedstrom, K. Aagaard, R. Woodgate, E. Curchitser, and P. Stabeno (2014), Ekman transport, continental shelf waves, and variations of the Pacific-Arctic sea surface height gradient: Coupled wind-forced controls of the Bering-Chukchi shelf circulation and the Bering Strait throughflow, *Progr. Oceanogr.*, *125*, 40–61.

Efron, B., and R. J. Tibshirani (1993), *An Introduction to the Bootstrap*, 436 pp., Chapman and Hall/CRC, New York.

Gawarkiewicz, G., and D. C. Chapman (1995), A numerical study of dense water formation and transport on a shallow, sloping continental shelf, *J. Geophys. Res.*, *100*, 4489–4508.

Gill, A. E., and E. H. Schumann (1974), The generation of long shelf waves by the wind, *J. Phys. Oceanogr.*, *4*, 83–90.

Gong, D., and R. S. Pickart (2015), Summertime circulation in the eastern Chukchi Sea, *Deep Sea Res., Part II*, *118*, 18–31.

Itoh, M., K. Shimada, T. Kamoshida, F. McLaughlin, E. Carmack, and S. Nishino (2012), Interannual variability of PWW inflow through Barrow Canyon from 2000 to 2006, *J. Oceanogr.*, *68*, 575–592, doi:10.1007/s10872-012-0120-1.

Itoh, M, S. Nishino, Y. Kawaguchi, and T. Kikuchi (2013), Barrow Canyon volume, heat, and freshwater fluxes revealed by long-term mooring observations between 2000 and 2008, *J. Geophys. Res.*, *118*, 4363–4379, doi:10.1002/jgrc.20290.

King, R. S., and B. Julstrom (1982), *Applied Statistics Using the Computer*, 477 pp. Alfred Publ. Co., Sherman Oaks, Calif.

Kohut, J. T., and S. Glenn (2003), Improving HF radar surface current measurements with measured antenna beam patterns, *J. Atmos. Oceanic Technol.*, *20*, 2303–1316.

Ladd, C., C. W. Mordy, S. A. Salo, and P. J. Stabeno (2016), Winter Water Properties and the Chukchi Polynya, *J. Geophys. Res. Oceans*, *121*, 5516–5534, doi:10.1002/2016JC011918.

Lu, P., Z. Li, B. Cheng, and M. Leppäranta (2011), A parameterization of the ice-ocean drag coefficient, *J. Geophys. Res.*, *116*, C07019, doi: 10.1029/2010JC006878.

Macready, P., and P. B. Rhines (1993), Slippery bottom boundary layers on a slope, *J. Phys. Oceanogr.*, *23*, 5–23.
Mesinger, F., et al. (2006), North American regional re-analysis, *Bull. Am. Meteorol. Soc.*, *87*, 343–360.
Mountain, D., L. Coachman, and K. Aagaard (1976), On the flow through Barrow Canyon, *J. Phys. Oceanogr.*, *6*, 461–470, doi:10.1175/1520-0485(1976)006 < 0461:OTFTBC>2.0.CO;2.
Mudge, T. D., et al. (2015), *Analysis of Ice and Metocean Measurements, Chukchi Sea 2013–2014, for Shell*, xi + 108 pp., Proj. Rep. for Shell Int. Explor. and Prod. Inc., Houston, Texas by ASL Environmental Sciences Inc., Victoria, B. C.
Münchow, A., and E. Carmack (1997), Synoptic flow and density observation near an Arctic Shelf Break, *J. Phys. Oceanogr.*, *27*, 1402–1419.
Nikolopoulos, A., R. S. Pickart, P. S. Fratantoni, K. Shimada, D. J. Torres, and E. P. Jones (2009), The western Arctic boundary current at 152°W: Structure, variability, and transport, *Deep Sea Res., Part II*, *56*, 1164–1181.
Nishino, S., T. Kikuchi, M. Yamamoto-Kawai, Y. Kawaguchi, T. Hirawake, and M. Itoh (2011), Enhancement/reduction of biological pump depends on ocean circulation in the sea-ice reduction regions of the Arctic Ocean, *J. Oceanogr.*, *67*, 305–314, doi:10.1007/s10872-011-0030-7.
Nof, D. (1988), Outflows dynamics, *Geophys. Astrophys. Fluid Dyn.*, *40*, 165–193.
Nof, D. (1991), Lenses generated by intermittent currents, *Deep Sea Res., Part A*, *38*(3), 325–345.
Pickart, R., T., Weingartner, L. Pratt, S. Zimmermann, and D. Torres (2005), Flow of winter-transformed Pacific water into the Western Arctic, *Deep Sea Res., Part II*, *52*, 3175–3198.
Pickart, R. S. (2004), Shelfbreak circulation in the Alaskan Beaufort Sea: Mean structure and variability, *J. Geophys. Res.*, *109*, C04024, doi: 10.1029/2003JC001912.
Pickart, R. S., G. W. K. Moore, C. Mao, F. Bahr, C. Nobre, and T. J. Weingartner (2016), Circulation of winter water on the Chukchi shelf in early Summer, *Deep Sea Res., Part II*, *130*, 46–75, doi:10.1016/j.dsr2.2016.05.001.
Schulze, L. M., and R. S. Pickart (2012), Seasonal variation of upwelling in the Alaskan Beaufort Sea: Impact of sea ice cover, *J. Geophys. Res.*, *117*, C06022, doi:10.1029/2012JC007985.
Shimada, K., M. Itoh, and S. Nishino (2005), Halocline structure in the Canada Basin of the Arctic Ocean, *Geophys. Res. Lett.*, *32*, L03605, doi: 10.1029/2004GL021358.
Shimada, K., T. Kamoshida, M. Itoh, S. Nishino, E. Carmack, F. McLaughlin, S. Zimmermann, and A. Proshutinsky (2006), Pacific Ocean inflow: Influence on catastrophic reduction of sea ice cover in the Arctic Ocean, *Geophys. Res. Lett.*, *33*, L08605, doi:10.1029/2005GL025624.
Shroyer, E. L. (2012), Turbulent kinetic energy dissipation in Barrow Canyon, *J. Phys. Oceanogr.*, *42*, 1012–1021.
Shroyer, E. L., and A. J. Plueddemann (2012), Wind-driven modification of the Alaskan coastal current, *J. Geophys. Res.*, *117*, C03031, doi: 10.1029/2011JC007650.
Signorini, S. R., A. Münchow, and D. Haidvogel (1997), Flow dynamics in a wide Arctic canyon, *J. Geophys. Res.*, *102*, 18,661–18,680.
Spall, M. A. (2007), Circulation and water mass transformation in a model of the Chukchi Sea, *J. Geophys. Res.*, *112*, C05025, doi:10.1029/2005JC002264.
Spall, M. A. (2013), On the circulation of Atlantic Water in the Arctic Ocean, *J. Phys. Oceanogr.*, *43*, 2352–2371.
Spall, M., R. S. Pickart, P. Fratantoni, and A. Plueddemann (2008), Western Arctic Shelfbreak Eddies: Formation and transport, *J. Phys. Oceanogr.*, *38*, 1644–1668.
Spall, M. A., R. S. Pickart, E. T. Brugler, G. W. K. Moore, L. Thomas, and K. R. Arrigo (2014), Role of shelfbreak upwelling in the formation of a massive under-ice bloom in the Chukchi Sea, *Deep Sea Res., Part II*, *105*, 17–29.
Steele, M., J. Morison, W. Ermold, I. Rigor, M. Orrmeyer, and K. Shimada (2004), Circulation of summer Pacific halocline water in the Arctic Ocean, *J. Geophys. Res.*, *109*, C02029, doi:10.1029/2003JC002009.
Walsh, J. J., et al. (1989), Carbon and nitrogen cycling within the Bering/Chukchi seas: Source regions for organic matter affecting AOU demands of the Arctic Ocean, *Prog. Oceanogr.*, *22*, 277–359.
Watanabe, E. (2011), Beaufort shelf break eddies and shelf-basin exchange of Pacific summer water in the western Arctic Ocean detected by satellite and modeling analyses, *J. Geophys. Res.*, *116*, C08034, doi:10.1029/2010JC006259.
Weingartner, T., D. Cavalieri, K. Aagaard, and Y. Sasaki (1998), Circulation, dense water formation, and outflow on the northwest Chukchi shelf, *J. Geophys. Res.*, *103*, 7647–7661.
Weingartner, T., K. Aagaard, R. Woodgate, S. Danielson, Y. Sasaki, and D. Cavalieri (2005), Circulation on the north central Chukchi Sea shelf, *Deep Sea Res., Part II*, *52*, 3150–3174.
Weingartner, T., P. Winsor, R. Potter, H. Statscewich, and E. Dobbins (2013a), Application of high frequency radar to potential hydrocarbon development areas in the northeast Chukchi sea, 165 pp., *Final Rep. BOEM Contract M09AC15207*, Bur. of Ocean Energy Manage., Anchorage, Alaska.
Weingartner, T., E. Dobbins, S. Danielson, R. Potter, H. Statscewich, and P. Winsor (2013b), Hydrographic variability over the northeastern Chukchi Sea shelf in summer-fall 2008–2010, *Cont. Shelf Res.*, *67*, 5–22, doi:10.1016/j.csr.2013.03.012.
Winsor, P., and D. C. Chapman (2002), Distribution and interannual variability of dense water production from coastal polynyas on the Chukchi Shelf, *J. Geophys. Res.*, *107*, 16-1–16-15, doi:10.1029/2001JC000984.
Winsor, P., and D. C. Chapman (2004), Pathways of Pacific Water across the Chukchi Sea: A numerical model study, *J. Geophys. Res.*, *109*, C03002, doi:1029/2003JC001962.
Woodgate, R., K. Aagaard, and T. Weingartner (2005a), A year in the physical oceanography of the Chukchi Sea: Moored measurement from autumn 1990–1991, *Deep Sea Res., Part II*, *52*, 3116–3149.
Woodgate, R., K. Aagaard, and T. Weingartner (2005b), Monthly temperature, salinity, and transport of the Bering Strait flow, *Geophys. Res. Lett.*, *32*, L04601, doi:10.1029/2004GL021880.
Woodgate, R., T. Weingartner, and R. Lindsay (2010), The 2007 Bering Strait ocean heat flux and anomalous Arctic sea-ice retreat, *Geophys. Res. Lett.*, *37*, L01602, doi:10.1029/2009GL041621.
Yamamoto-Kawai, F. McLaughlin, E. Carmack, S. Nishino, and K. Shimada (2008), Freshwater budget of the Canada Basin, Arctic Ocean, from salinity, δ^{18}O, and nutrients, *J. Geophys. Res.*, *113*, C01007, doi:10.1029/2006JC003858.
Zhao, M., M.-L. Timmermans, S. Cole, R. Krishfield, A. Proshutinsky, and J. Toole (2014), Characterizing the eddy field in the Arctic Ocean halocline, *J. Geophys. Res. Oceans*, *119*, 8800–8817, doi:10.1002/2014JC010488.